Celest Mech Dyn Astr (2011) 110:71–98
DOI 10.1007/s10569-011-9340-8

ORIGINAL ARTICLE

On quasi-periodic motions around the collinear libration points in the real Earth–Moon system

X. Y. Hou · L. Liu

Received: 17 September 2010 /Revised: 6 March 2011 / Accepted: 10 March 2011 /
Published online: 10 April 2011

Abstract Due to various perturbations, the collinear libration points of the real Earth–Moon system are not equilibrium points anymore. Under the assumption that the Moon's motion is quasi-periodic, special quasi-periodic orbits called dynamical substitutes exist. These dynamical substitutes replace the geometrical collinear libration points as time-varying equilibrium points. In the paper, the dynamical substitutes of the three collinear libration points in the real Earth–Moon system are computed. For the points L_1 and L_2, linearized motions around the dynamical substitutes are described, and the variational equations of the dynamical substitutes are reduced to a form with a near constant coefficient matrix. Then higher order analytical formulae of the central manifolds are constructed. Using these analytical solutions as initial seeds, Lissajous orbits and halo orbits are computed with numerical algorithms.

Keywords Earth–Moon system · Collinear libration point · Dynamical substitute · Lissajous orbit · Halo orbit · Quasi-periodic orbits

1 Introduction

Since Clark proposed the use of collinear libration points (Dunham and Farquhar 2003), an upsurge of utilizing these points in space missions arises. Till now, several missions have utilized collinear libration points of the Sun–Earth system, such as ISEE-3, ACE, GENESIS

X. Y. Hou (✉) · L. Liu
Astronomy Department, Nanjing University, 210093 Nanjing, China
e-mail: silence@nju.edu.cn

X. Y. Hou · L. Liu
Institute of Space Environment and Astrodynamics, Nanjing University, 210093 Nanjing, China

X. Y. Hou · L. Liu
Key Laboratory of Modern Astronomy and Astrophysics, Ministry of Education, Nanjing University, 210093 Nanjing, China

and PLANCK. More future missions will be sent to these points. Besides the Sun–Earth system, collinear libration points of the Earth–Moon system are also being considered for some space missions (Folda and Vaughn 2004; Broschart et al. 2009; Romagnoli and Circi 2010).

The dynamics of the collinear libration points, which are crucial to these missions, have been carefully studied. Take these works (Gómez et al. 2001a,b; Farrés and Jorba 2010) as a few examples. The most studied model is the circular restricted three-body problem (CRTBP). For some restricted problems in the Solar System, this model is a good approximation. But for some restricted problems, this model is not satisfactory enough. An example is the Earth–Moon system. Perturbations from the Moon's orbit eccentricity and from the Sun are so large that they should be taken into consideration when designing missions in this system.

For the real Earth–Moon system, the three collinear libration points are in fact not equilibrium points anymore, only retaining their geometrical meanings. Special quasi-periodic orbits around them exist. These orbits substitute the geometrical libration points as time-varying equilibrium points. They are often called dynamical substitutes. The dynamical substitutes of the triangular libration points in the real Earth–Moon system were computed before (Díez et al. 1991; Gómez et al. 2001c,d; Hou and Liu 2010). For the collinear libration points, their dynamical substitutes were also computed for some simplified models of the real Earth–Moon system (Andreu 1998; Gómez et al. 2002). Using the method proposed in (Hou and Liu 2010), the dynamical substitutes of the three collinear libration points in the real Earth–Moon system are computed in this paper.

After we obtain these dynamical properties, their dynamical properties are studied. It turns out that they are all unstable, but with central manifolds around them. For the points L_1 and L_2, linearized motions around the dynamical substitutes are analyzed with the aid of FFT analysis. Then the variational equations of the dynamical substitutes are reduced to a form with a near constant coefficient matrix. With this reduced form, we're able to construct higher order analytical solutions of the central manifolds. Using these high order analytical solutions as initial seeds, Lissajous orbits and halo orbits lasting quite a long time are constructed with numerical algorithms. The reason why we only study the motions around the points L_1 and L_2 lies in the fact that these two points are the interests of people for future space missions but the point L_3 is not.

In the paper, when we refer to the real Earth–Moon system, we mean the gravitational model of the nine planets (including Pluto), the Moon and the Sun. Their motions are given by the ephemeris. The numerical ephemeris JPL DE406 is used. Denote the set of these major bodies as $S = (\mu_1, \ldots, \mu_{11})$, where $\mu_1 \sim \mu_9$ indicate the reduced masses of the nine planets and μ_{10}, μ_{11} indicate the reduced masses of the Moon and the Sun. $\mu_i = m_i/(m_3 + m_{10})$, where $m_i (i = 1, \ldots, 11)$ are the masses of the nine planets, the Moon and the Sun. The mass unit is the sum of the masses of the Earth and the Moon $[M] = m_3 + m_{10}$. The length unit $[L] = 384747981$ m is the mean distance between the Earth and Moon. The time unit is $[T] = 375699.843898365$ s. These are the units used in the following dynamical equations.

2 Dynamical equations

In the Earth-centered synodic coordinate, the small body follows (Hou and Liu 2010)

$$\ddot{\mathbf{r}} = -2C^T\dot{C}\dot{\mathbf{r}} - C^T\ddot{C}\mathbf{r} - \mu_3\mathbf{r}/r^3 - \sum_{i\in S, i\neq 3} \mu_i \left(\boldsymbol{\delta}_i/\delta_i^3 + \mathbf{r}_i/r_i^3\right), \tag{1}$$

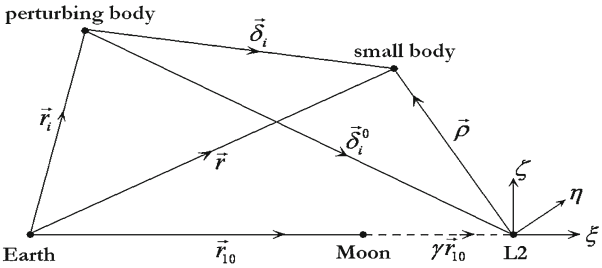

Fig. 1 An illustration picture of the vectors in Eqs. (1) and (5)

where $\mathbf{r}$ is the position of the small body, $\mathbf{r}_i$ is the position of the major body μ_i, and $\boldsymbol{\delta}_i = \mathbf{r} - \mathbf{r}_i$. The matrix C is

$$C = (\hat{e}_1, \hat{e}_2, \hat{e}_3); \quad \hat{e}_1 = \mathbf{R}_{10}/k, \quad \hat{e}_3 = (\mathbf{R}_{10} \times \dot{\mathbf{R}}_{10})/\|\mathbf{R}_{10} \times \dot{\mathbf{R}}_{10}\|, \quad \hat{e}_2 = \hat{e}_3 \times \hat{e}_1, \tag{2}$$

where $\mathbf{R}_{10}$ is the position of the Moon in an Earth-centered sidereal coordinate and $k = |\mathbf{R}_{10}|$. Denote the geometric position of the collinear libration point in the Earth-centered synodic coordinate as $\mathbf{r}_0$.

$$\mathbf{r}_0 = (1 + \gamma)\mathbf{r}_{10}, \tag{3}$$

The value of γ in Eq. (3) is -0.150934288618019 for the point L_1, 0.167832751054508 for the point L_2 and -1.992912060200654 for the point L_3. These values are obtained in the circular restricted three-body problem of the Earth–Moon system. The transformation

$$\mathbf{r} = \boldsymbol{\rho} + \mathbf{r}_0 \tag{4}$$

moves the origin from the Earth to the collinear libration point $\mathbf{r}_0$. Substituting Eq. (4) into Eq. (1), we obtain the motion equations in the collinear libration point centered synodic coordinate, in the form of

$$\begin{cases} \ddot{\boldsymbol{\rho}} = \mathbf{F}_1 + \mathbf{F}_2 \\ \mathbf{F}_1 = -2C^T\dot{C}\dot{\boldsymbol{\rho}} - C^T\ddot{C}\boldsymbol{\rho} - \mu_3\mathbf{r}/r^3 + \mu_3\mathbf{r}_0/r_0^3 - \sum\limits_{i\in S, i\neq 3}\mu_i\left[\boldsymbol{\delta}_i/\delta_i^3 - \boldsymbol{\delta}_i^0/\left(\delta_i^0\right)^3\right] \\ \mathbf{F}_2 = -\mu_3\mathbf{r}_0/r_0^3 - \sum\limits_{i\in S, i\neq 3}\mu_i\left[\boldsymbol{\delta}_i^0/\left(\delta_i^0\right)^3 + \mathbf{r}_i/r_i^3\right] - \ddot{\mathbf{r}}_0 - 2C^T\dot{C}\dot{\mathbf{r}}_0 - C^T\ddot{C}\mathbf{r}_0 \end{cases}, \tag{5}$$

where $\boldsymbol{\delta}_i^0 = \mathbf{r}_0 - \mathbf{r}_i$. Taking the collinear libration point L_2 as an example, Fig. 1 shows the relation of the vectors in the equations.

The term $\mathbf{F}_1$ can be expanded as a literal series of $\boldsymbol{\rho}, \dot{\boldsymbol{\rho}}$, being zero when $\boldsymbol{\rho}, \dot{\boldsymbol{\rho}} = 0$. Neglecting the very small planetary terms, this series is of the following form

$$\mathbf{F}_1 = -2C^T\dot{C}\dot{\boldsymbol{\rho}} - C^T\ddot{C}\boldsymbol{\rho} + \frac{\partial}{\partial\boldsymbol{\rho}}(\Omega_1 + \Omega_2 + \Omega_3), \tag{6}$$

in which

$$\begin{cases} \Omega_1 = \sum\limits_{n=2}^{\infty}\frac{\mu_3}{r_0}\left[\left(\frac{\rho}{r_0}\right)^n P_n\left(\cos\Psi_3'\right)\right] \\ \Omega_2 = \sum\limits_{n=2}^{\infty}\frac{\mu_{10}}{\delta_{10}^0}\left[\left(\frac{\rho}{\delta_{10}^0}\right)^n P_n\left(\cos\Psi_{10}'\right)\right] \\ \Omega_3 = \sum\limits_{n=2}^{\infty}\frac{\mu_{11}}{\delta_{11}^0}\left[\left(\frac{\rho}{\delta_{11}^0}\right)^n P_n\left(\cos\Psi_{11}'\right)\right] \end{cases}. \tag{7}$$

In the above equations, $\mu_3 = 0.987849414390376$ is the reduced mass of the Earth, $\mu_{10} = 0.012150585609624$ is the reduced mass of the Moon and $\mu_{11} = 328900.5614000000$ is the reduced mass of the Sun. Ψ_i' is the angle between the vector $\boldsymbol{\rho}$ and the vector δ_i^0.

The term $\mathbf{F}_2$ depends on the motion of the major bodies in the set S, irrelevant to $\boldsymbol{\rho}$, $\dot{\boldsymbol{\rho}}$. For the last three terms in $\mathbf{F}_2$, also neglecting the planetary terms, we have

$$\begin{aligned} -\ddot{\mathbf{r}}_0 - 2C^T\dot{C}\dot{\mathbf{r}}_0 - C^T\ddot{C}\mathbf{r}_0 &= -(1+\gamma)C^T\ddot{\mathbf{R}}_{10} \\ &= (1+\gamma)\left[\frac{\mathbf{r}_{10}}{r_{10}^3} + \mu_{11}\left(\frac{\boldsymbol{\delta}_{11,10}}{\delta_{11,10}^3} + \frac{\mathbf{r}_{11}}{r_{11}^3}\right)\right] \end{aligned} \tag{8}$$

where $\boldsymbol{\delta}_{11,10} = \mathbf{r}_{10} - \mathbf{r}_{11}$. Substituting Eq. (8) into $\mathbf{F}_2$, it's easy to prove that all the terms relevant to the Earth and the Moon disappear and only the terms relevant to the Sun remain

$$\mathbf{F}_2 = -\mu_{11}\left[\frac{\boldsymbol{\delta}_{11}^0}{\left(\delta_{11}^0\right)^3} + \frac{\mathbf{r}_{11}}{r_{11}^3}\right] + (1+\gamma)\mu_{11}\left[\left(\frac{\boldsymbol{\delta}_{11,10}}{\delta_{11,10}^3} + \frac{\mathbf{r}_{11}}{r_{11}^3}\right)\right] \tag{9}$$

We can rewrite $\mathbf{F}_2$ as

$$\begin{aligned} \mathbf{F}_2 &= \frac{\mu_{11}}{r_{11}}\sum_{n=3}^{\infty}\left\{\frac{\partial}{\partial \mathbf{r}_0}\left[\left(\frac{r_0}{r_{11}}\right)^n P_n(\cos\Psi)\right] - (1+\gamma)\frac{\partial}{\partial \mathbf{r}_{10}}\left[\left(\frac{r_{10}}{r_{11}}\right)^n P_n(\cos\Psi)\right]\right\} \\ &\sim |\gamma+\gamma^2|\frac{\mu_{11}}{r_{11}^4} \end{aligned} \tag{10}$$

where Ψ is the angle between the Moon's and the Sun's vectors with respect to the Earth.

Due to the existence of the term $\mathbf{F}_2$ in Eq. (5), the collinear libration point expressed as $\boldsymbol{\rho}, \dot{\boldsymbol{\rho}} = 0$ is not an equilibrium point. The term $\mathbf{F}_2$ and the coefficients in the literal series of $\mathbf{F}_1$ are relevant to the Moon's motion. They are quasi-periodic under the assumption that the Moon's motion is quasi-periodic. A basic frequency set W exists for these quasi-periodic functions. Similar to the triangular libration points (Díez et al. 1991; Gómez et al. 2001c,d), special quasi-periodic orbits around the collinear libration points exist as their dynamical substitutes. These quasi-periodic orbits only contain frequencies that are linear combinations of the elements in the set W. Neglecting the planetary terms, the set W contains 4 elements (Hou and Liu 2010)

$$\begin{aligned} &\omega_1 = 0.99154828857, \quad \omega_2 = 0.07480066375, \quad \omega_3 = 0.92519871658, \\ &\omega_4 = 1.00402177967. \end{aligned}$$

The magnitude of the term $\mathbf{F}_2$ in Eq. (10) indicates that the amplitude of the dynamical substitute is very small, which is supported by our studies.

3 The dynamical substitutes

Equation (5) can be written as (Hou and Liu 2010)

$$\begin{cases} \ddot{\xi} = c_1 + c_4\dot{x} + c_5\dot{y} + \sum\limits_{ijk}\xi_{ijk}x^i y^j z^k \\ \ddot{\eta} = c_2 - c_5\dot{x} + c_4\dot{y} + c_6\dot{z} + \sum\limits_{ijk}\eta_{ijk}x^i y^j z^k, \quad i,j,k \geq 0, \quad i+j+k \geq 1 \\ \ddot{\zeta} = c_3 - c_6\dot{y} + c_4\dot{z} + \sum\limits_{ijk}\zeta_{ijk}x^i y^j z^k \end{cases} \tag{11}$$

where $c_1 \sim c_6, \xi_{ijk}, \eta_{ijk}, \zeta_{ijk}$ are quasi-periodic functions with the basic frequency set W. These coefficients are first analyzed with FFT methods. Then the linearized equation of Eq. (11) can be solved. By adding higher order terms to the motion equations, higher order analytical approximations of the dynamical substitutes can be obtained (Díez et al. 1991; Gómez et al. 2001c,d). The dynamical substitutes of the three collinear libration points are expressed as

$$\begin{cases} \bar{\xi} = \sum\limits_{i,j,k,l} \bar{C}_{ijkl} \cos[(i\omega_1 + j\omega_2 + k\omega_3 + l\omega_4)t] + \bar{S}_{ijkl} \sin[(i\omega_1 + j\omega_2 + k\omega_3 + l\omega_4)t] \\ \bar{\eta} = \sum\limits_{i,j,k,l} \bar{C}'_{ijkl} \cos[(i\omega_1 + j\omega_2 + k\omega_3 + l\omega_4)t] + \bar{S}'_{ijkl} \sin[(i\omega_1 + j\omega_2 + k\omega_3 + l\omega_4)t] \\ \bar{\zeta} = \sum\limits_{i,j,k,l} \bar{C}''_{ijkl} \cos[(i\omega_1 + j\omega_2 + k\omega_3 + l\omega_4)t] + \bar{S}''_{ijkl} \sin[(i\omega_1 + j\omega_2 + k\omega_3 + l\omega_4)t] \end{cases} \tag{12}$$

Due to the infinity of the series, we're only able to collect the terms larger than a fixed amplitude in the series. In our work, this value is set to be 1×10^{-8} (dimensionless unit) for the points L_1, 1×10^{-7} (dimensionless unit) for the point L_2 and 2×10^{-6} (dimensionless unit) for the point L_3.

In fact, we didn't take the method described in Díez et al. (1991); Gómez et al. (2001c,d). The algorithm in Hou and Liu (2010) was used. Here is a brief description of the algorithm.

With the aid of the parallel shooting method (Gómez et al. 2001b), quasi-periodic orbits around the collinear libration points lasting a long time can be constructed. In our work, the time interval between consecutive nodal points is 0.8 dimensionless units (about 3.4787 days). Totally, 65537 nodal points are used and the constructed orbit lasts about 624 years. Equation (1) is used for all the integrations in this paper. The initial seed of the first quasi-periodic orbit constructed is the collinear libration point itself. This quasi-periodic orbit is in fact one member of the central manifolds around the dynamical substitute. FFT analysis is applied to this quasi-periodic orbit to obtain its frequencies. The time interval between the sampling data is 0.1 dimensionless units. Totally $N = 2^{19}$ sampling data were used. The same interval and N are taken for all the FFT analysis in the following discussions.

Studies show that there are some frequencies that can not be expressed as linear combinations of the members in the set W. Another two basic frequencies v_1 and v_2 exist and the frequencies of the quasi-periodic orbit are of the form

$$\omega = i\omega_1 + j\omega_2 + k\omega_3 + l\omega_4 + mv_1 + nv_2, \tag{13}$$

where i, j, k, l, m, n are integers and $i \geq 0$. This indicates that there are two components of the central manifolds. Obviously, the amplitudes of the two frequencies $i = j = k = l = n = 0, m = 1$ and $i = j = k = l = m = 0, n = 1$ are the amplitudes of the two central components. Denote them as γ_1 and γ_2. Take the ξ component as an example. Denote the coefficients of the terms with $m = n = 0$ as $C^{(1)}_{ijkl00}$ and $S^{(1)}_{ijkl00}$. According to the discussions on the central manifolds below, the difference between $C^{(1)}_{ijkl00}$, $S^{(1)}_{ijkl00}$ and $\bar{C}_{ijkl}$, $\bar{S}_{ijkl}$ in Eq. (12) is of the order γ_1^2 or γ_2^2. Take $C^{(1)}_{ijkl00}$, $S^{(1)}_{ijkl00}$ as approximations of $\bar{C}_{ijkl}$, $\bar{S}_{ijkl}$ and substitute them into Eq. (12), a better initial seed than the collinear libration point itself can be used for the parallel shooting method. The resulting quasi-periodic orbit should be closer to the dynamical substitute. We analyze the newly computed quasi-periodic orbit to obtain the coefficients $C^{(2)}_{ijkl00}$, $S^{(2)}_{ijkl00}$, repeat the above steps and gradually approach the dynamical substitute. In our studies, this algorithm works very well. For all the three collinear libration points, only one iteration is enough to obtain the accuracy required. The results will be stated below.

3.1 The numerical results

(1) the point L_1

Studies show that the two basic frequencies of the central manifolds are $v_1 \approx 2.3377$ and $v_2 \approx 2.2743$. We manage to obtain a quasi-periodic orbit with $\gamma_1, \gamma_2 < 10^{-8}$. Practically speaking, this quasi-periodic orbit can be taken as the true dynamical substitute. Figure 2 shows this dynamical substitute, starting from the epoch MJD = 51544.5000 and lasting about 624 years. The unit of the coordinate is $[L]/10^6 = 384.747981$ m. The dynamical substitute is actually a smooth quasi-periodic orbit. The discontinuities shown in the figures are due to the accumulation of thousands and thousands of loops. The orbit shown in the figure is constructed using the parallel shooting method, with the time interval between two consecutive nodal points equaling 0.8 dimensionless units (same for the points L_2 and L_3).

(2) the point L_2

The results of L_2 are similar to those of L_1. The two basic frequencies of the central manifolds are $v_1 \approx 1.8646$ and $v_2 \approx 1.7909$. We manage to obtain a quasi-periodic orbit with $\gamma_1, \gamma_2 < 10^{-8}$ and take it as an approximation of the true dynamical substitute. Figure 3 shows the dynamical substitute, also starting from the epoch MJD = 51544.5000 and lasting about 624 years. The unit of the coordinate is $[L]/10^5 = 3847.47981$ m.

(3) the point L_3

The results of L_3 are similar to those of L_1 and L_2. The two basic frequencies of the central manifolds are $v_1 \approx 1.0031$ and $v_2 \approx 1.0093$. We manage to obtain a quasi-periodic orbit with $\gamma_1, \gamma_2 < 10^{-8}$ and take it as an approximation of the true dynamical substitute. Figure 4 shows the dynamical substitute. Also starting from the epoch MJD = 51544.5000 and lasting about 624 years. The unit of the coordinate is $[L]/10^3 = 384747.981$ m.

Figure 5 shows the deviation between the analytic solution given by Eq. (12) and the numerically integrated orbit. The initial condition of the integrated orbit is the same as the one used for the analytic solution. To save space, we only give the projections of the two orbits on the $x - y$ plane. The dashed curve is the analytic orbit and the solid curve is the integrated orbit. The starting epoch is MJD = 51544.5000. The left frame is for the point L_1. The integrated time is 6.9574 days. The middle frame is for the point L_2. The integrated time

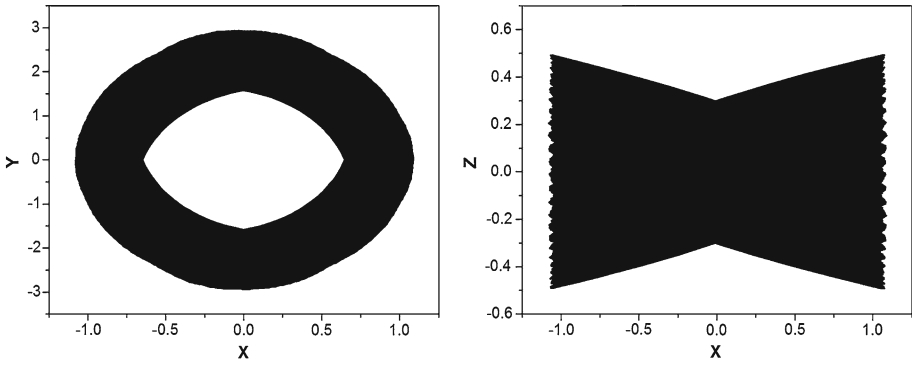

Fig. 2 The dynamical substitute of L_1 (projections on the $x - y$ and $x - z$ planes). The unit of the coordinate is $[L]/10^6 = 384.747981$ m

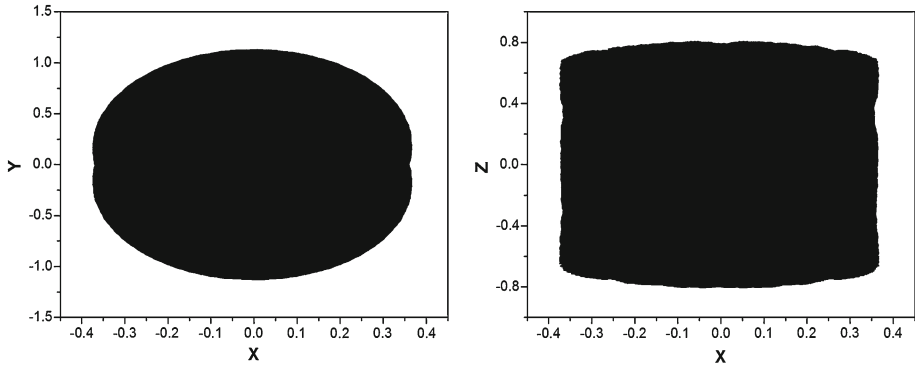

Fig. 3 The dynamical substitute of L_2 (projections on the $x-y$ and $x-z$ planes). The unit of the coordinate is $[L]/10^5 = 3847.47981$ m

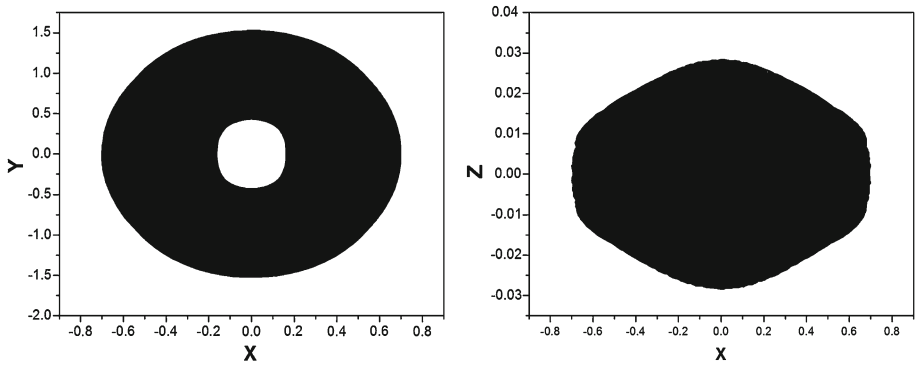

Fig. 4 The dynamical substitute of L_3 (projections on the $x-y$ and $x-z$ planes). The unit of the coordinate is $[L]/10^3 = 384747.981$ m

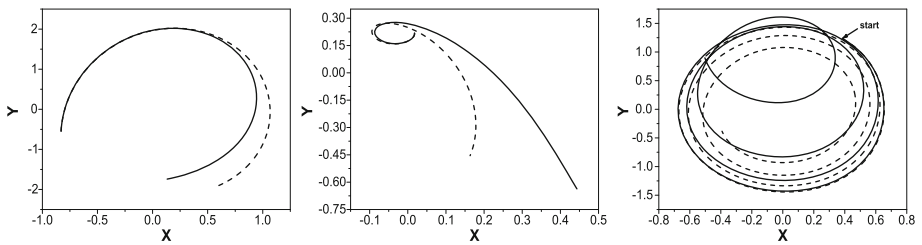

Fig. 5 Deviations between the analytic dynamical substitute (*dashed line*) and the integrated orbit (*solid line*). The analytic orbit and the integrated orbit have same initial conditions. From left to right, for the points L_1, L_2, L_3, respectively. The unit of the coordinate is $[L]/10^6 = 384.747981$ m for the *left frame*, $[L]/10^5 = 3847.47981$ m for the *middle frame* and $[L]/10^3 = 384747.981$ m for the *right frame*

is 10.4361 days. The right frame is for the point L_3. The integrated time is 104.3611 days. Compared with the points L_1, L_2, the instability of L_3 is obviously much milder.

In order to check the results, Table 1 shows one primary periodic term of the dynamical substitute for each collinear libration point, expressed in dimensionless units. Readers who are interested in the full numerical results can write to the authors for the whole tables.

Table 1 One primary periodic term for each dynamical substitute of the three collinear libration points

Component	ω_1	ω_2	ω_3	ω_4	c_ω	s_ω
$L_1 - x$	0	0	3	0	−0.000000842316201	−0.000000094581265
$L_1 - y$	0	0	3	0	−0.000000257253110	0.000002291046236
$L_1 - z$	0	0	1	1	0.000000102630575	0.000000169735329
$L_2 - x$	−1	0	3	0	−0.000001149332358	0.000000920308794
$L_2 - y$	−1	0	3	0	0.000002975227681	0.000003715539811
$L_2 - z$	0	0	3	−1	0.000006397227461	0.000001093628951
$L_3 - x$	0	0	1	0	0.000203081096344	0.000384119997422
$L_3 - y$	0	0	1	0	0.000834610192243	−0.000441231830494
$L_3 - z$	0	0	−1	1	−0.000002745039653	0.000006003588074

Table 2 Discontinuities of each step in computing the dynamical substitutes

Iterations	0	1	2	3	4
L_1	0.00228576	0.00000521	$< 1 \times 10^{-8}$	–	–
L_2	0.00837961	0.00006963	$< 1 \times 10^{-8}$	–	–
L_3	0.36850616	0.09922195	0.00895571	0.00007949	$< 1 \times 10^{-8}$

Taking these analytical solutions as initial seeds, the parallel shooting method can be used to generate quasi-periodic orbits which are very close to them. Table 2 shows the discontinuity (including position and velocity) of the total nodal points in each iterations. The iteration process is stopped when the discontinuity is smaller than 1×10^{-8}. The total number of the nodal points is 65537. This means the average discontinuity at each nodal point is of the order 10^{-13}.

Generally, the dynamical substitute is unstable. Denote $\Delta X(t)$ as the deviation between the dynamical substitute and an orbit around it. In order to keep the orbit within the proximity of the dynamical substitute, every after a fixed time Δt, we reset the initial condition of the orbit. An illustration picture is shown in Fig. 6. At the time $t_{i-1} = (i-1)\Delta t$, we reset ΔX_{i-1} as $\Delta X'_{i-1} = \Delta X_{i-1} \cdot d_0 / \parallel \Delta X_{i-1} \parallel$ to start the new orbit segment. $d_i = \parallel \Delta X_i \parallel$ and d_0 is the norm of the initial deviation at the starting time t_0. This is a typical method to compute the maximum Lyapunov exponent (Lichtenberg and Lieberman 1983). The maximum Lyapunov exponent is given by the following formula

$$v_3 = \lim_{n\to\infty} \sum_{i=1}^{n} \frac{\ln(d_i/d_0)}{n\Delta t}. \tag{14}$$

The length of the orbit segment Δt should be appropriately chosen so that the integrated orbit is within the proximity of the dynamical substitute. Take the point L_1 as example, the left frame of Fig. 7 shows the results corresponding to $\Delta t = 0.8$ dimensionless unit, starting from the epoch MJD = 51544.5000. The initial deviation is set to be $(10^{-6}, 0, 0, 0, 0, 0)^T$ dimensionless units. Similar choices go for the points L_2 and L_3. The width of the curves is due to the heavy density of the nodal points and periodic vibrations of the curve. The right frame shows the results corresponding to $\Delta t = 0.4$ dimensionless unit. Obviously, the value of the computed v_3 is approaching a critical value. This value is different if we choose

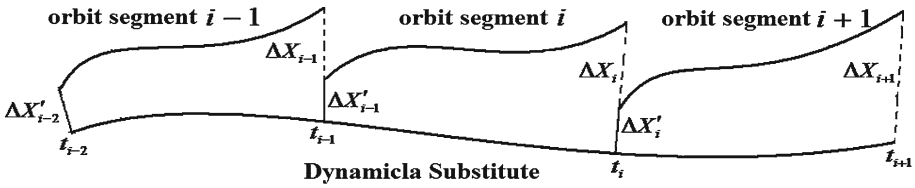

Fig. 6 An illustration picture of the way to compute the maximum Lyapunov exponent

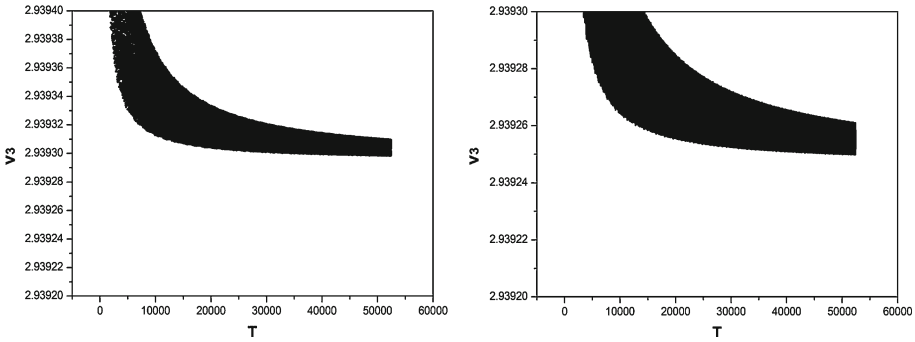

Fig. 7 The *curves* of the computed v_3. The abscissa is the time, expressed in dimensionless units. The *left frame* corresponds to the result of $\Delta t = 0.8$ dimensionless units and totally 65536 orbit segments are used. The *right frame* corresponds to the result of $\Delta t = 0.4$ dimensionless units and totally 131072 orbit segments are used

different Δt but they are very close. Since we only have a finite length of data, we are not able to obtain the accurate value. Considering the decreasing tendency of the curves with increasing length of data, we speculate $v_3 \approx 2.9392$. The first four figures of v_3 should be accurate. The last figure is a speculation. For the points L_2 and L_3, the computed maximum Lyapunov exponent are 2.1648 and 0.1798, respectively.

3.2 Comparison with previous results

Denoting the variables with a prime as the corresponding variables in the synodic coordinate centered at the barycenter of the Earth–Moon system, the transformation

$$\mathbf{r} = \mathbf{r}' + \mu_{10}\mathbf{r}_{10} \tag{15}$$

moves the origin from the Earth to the barycenter. Substituting Eq. (15) into (1) and neglecting the planetary terms, we obtain

$$\begin{aligned}\ddot{\mathbf{r}}' = &-2C^T\dot{C}\dot{\mathbf{r}}' - C^T\ddot{C}\mathbf{r}' - \mu_3\mathbf{r}/r^3 - \mu_{10}\boldsymbol{\delta}_{10}/\delta_{10}^3 - \mu_{11}\boldsymbol{\delta}_{11}/\delta_{11}^3 \\ &-\mu_3\mu_{11}\mathbf{r}_{11}/r_{11}^3 + \mu_{10}\mu_{11}\boldsymbol{\delta}_{11,10}/\delta_{11,10}^3.\end{aligned} \tag{16}$$

Under the assumption that the Moon's orbit is circular and

$$-\mu_3\mu_{11}\mathbf{r}_{11}/r_{11}^3 + \mu_{10}\mu_{11}\boldsymbol{\delta}_{11,10}/\delta_{11,10}^3 \approx -\mu_{11}\mathbf{r}'_{11}/r'^3_{11}, \tag{17}$$

Eq. (16) reduces to

$$\ddot{\mathbf{r}}' = 2\begin{pmatrix}\dot{y}' \\ x' \\ 0\end{pmatrix} + \begin{pmatrix}x' \\ y' \\ 0\end{pmatrix} - \mu_3\mathbf{r}/r^3 - \mu_{10}\boldsymbol{\delta}_{10}/\delta_{10}^3 - \mu_{11}\boldsymbol{\delta}_{11}/\delta_{11}^3 - \mu_{11}\mathbf{r}'_{11}/r'^3_{11}. \tag{18}$$

Under another assumption that the orbit of the Earth–Moon's barycenter around the Sun is also circular and coplanar with the Moon's orbit, Eq. (18) is the widely used bi-circular problem (Szebehely 1967; Gómez et al. 2001c).

The transformation

$$\mathbf{r}' = \boldsymbol{\rho} + \mathbf{r}'_0 = \boldsymbol{\rho} + (\mu_3 + \gamma)\mathbf{r}_{10} \tag{19}$$

moves the origin from the barycenter to the collinear libration point. $\mathbf{r}'_0 = (\mu_3+\gamma)\mathbf{r}_{10}$ is the position vector of the collinear libration point in the barycenter-centered synodic coordinate. Substituting Eq. (19) into (16), we have

$$\begin{cases} \ddot{\boldsymbol{\rho}} = \mathbf{F}_1 + \mathbf{F}_2 \\ \mathbf{F}_1 = -2C^T\dot{C}\dot{\boldsymbol{\rho}} - C^T\ddot{C}\boldsymbol{\rho} - \mu_3\mathbf{r}/r^3 + \mu_3\mathbf{r}_0/r_0^3 \\ \qquad -\mu_{10}\left[\boldsymbol{\delta}_{10}/\delta_{10}^3 - \boldsymbol{\delta}_{10}^0/\left(\delta_{10}^0\right)^3\right] - \mu_{11}\left[\boldsymbol{\delta}_{11}/\delta_{11}^3 - \boldsymbol{\delta}_{11}^0/\left(\delta_{11}^0\right)^3\right], \\ \mathbf{F}_2 = -\mu_3\mathbf{r}_0/r_0^3 - \mu_{10}\boldsymbol{\delta}_{10}^0/(\delta_{10}^0)^3 - \mu_{11}\boldsymbol{\delta}_{11}^0/\left(\delta_{11}^0\right)^3 \\ \qquad -\mu_3\mu_{11}\mathbf{r}_{11}/r_{11}^3 + \mu_{10}\mu_{11}\boldsymbol{\delta}_{11,10}/\delta_{11,10}^3 - \ddot{\mathbf{r}}'_0 - 2C^T\dot{C}\dot{\mathbf{r}}'_0 - C^T\ddot{C}\mathbf{r}'_0 \end{cases} \tag{20}$$

Neglecting the planetary terms, it's easy to prove that Eq. (20) is the same as Eq. (5). This is obvious because we are dealing with the same system described by Eq. (1). Equation (5) is obtained by directly moving the origin to the collinear libration point. Equation (20) is obtained by first moving the origin to the barycenter and then to the collinear libration point. Similar to Eq. (8), the following relation holds

$$\begin{aligned} -\ddot{\mathbf{r}}'_0 - 2C^T\dot{C}\dot{\mathbf{r}}'_0 - C^T\ddot{C}\mathbf{r}'_0 &= -(\mu_3+\gamma)C^T\ddot{\mathbf{R}}_{10} \\ &= (\mu_3+\gamma)\left[\frac{\mathbf{r}_{10}}{r_{10}^3} + \mu_{11}\left(\frac{\boldsymbol{\delta}_{11,10}}{\delta_{11,10}^3} + \frac{\mathbf{r}_{11}}{r_i^{11}}\right)\right]. \end{aligned} \tag{21}$$

However, for the BCP model, this transformation produces

$$-\ddot{\mathbf{r}}'_0 - 2C^T\dot{C}\dot{\mathbf{r}}'_0 - C^T\ddot{C}\mathbf{r}'_0 = -(\mu_3+\gamma)C^T\ddot{C}\mathbf{r}_{10} = (\mu_3+\gamma)(x_{10}, y_{10}, 0)^T \tag{22}$$

Noting the fact that for the BCP model, $r_{10} = (x_{10}, y_{10}, z_{10})^T = (1, 0, 0)^T$, Eq. (22) is the first term in Eq. (21). This means the BCP model can not produce the second term in Eq. (21) which comes from the Sun's perturbation. Due to this difference, the magnitude of the term $\mathbf{F}_2$ for the BCP model is of the magnitude μ_{11}/r_{11}^3, much larger than the one in Eq. (10). Compared with the BCP model, Eq. (5) or Eq. (20) can better describe the motions around the collinear libration points in the real Earth–Moon system.

In Andreu (1998), an improved model called quasi bi-circular problem (QBCP) was used. The author considered the effects of the Sun on the motion of the Moon. He first solved the coplanar three body problem of the Earth, the Moon and the Sun, and then obtained the coefficients $\alpha_1 \sim \alpha_6$ which are periodic functions with the basic frequency ω_3. The motion equations of the small body in the Earth–Moon barycenter centered synodic coordinate can be expressed as

$$\begin{cases} \ddot{x}' = -\alpha_1\alpha_4 + \frac{\dot{\alpha}_1}{\alpha_1}\dot{x}' + 2\alpha_3\dot{y}' + \left(\alpha_2^2 + \alpha_3^2 - \frac{\alpha_2}{\alpha_1}\dot{\alpha}_1 + \dot{\alpha}_2\right)x' + \left(\dot{\alpha}_3 - \frac{\alpha_3}{\alpha_1}\dot{\alpha}_1\right)y' + \alpha_1\alpha_6\frac{\partial\Omega}{\partial x'} \\ \ddot{y}' = -\alpha_1\alpha_5 - 2\alpha_3\dot{x}' + \frac{\dot{\alpha}_1}{\alpha_1}\dot{y}' - \left(\dot{\alpha}_3 - \frac{\alpha_3}{\alpha_1}\dot{\alpha}_1\right)x' + \left(\alpha_2^2 + \alpha_3^2 - \frac{\alpha_2}{\alpha_1}\dot{\alpha}_1 + \dot{\alpha}_2\right)y' + \alpha_1\alpha_6\frac{\partial\Omega}{\partial y'} \\ \ddot{z}' = \frac{\dot{\alpha}_1}{\alpha_1}\dot{z}' + \left(\alpha_2^2 + \dot{\alpha}_2 - \frac{\alpha_2}{\alpha_1}\dot{\alpha}_1\right)z' + \alpha_1\alpha_6\frac{\partial\Omega}{\partial z'} \end{cases} \tag{23}$$

For comparison with the following results, we rewrite Eq. (23) as

$$\begin{cases} \ddot{x}' = \bar{b}_1 + \bar{b}_4\dot{x}' + \bar{b}_5\dot{y}' + \bar{b}_7x' + \bar{b}_8y' + \bar{b}_9z' + \bar{b}_{13}\frac{\partial\Omega}{\partial x'} \\ \ddot{y}' = \bar{b}_2 - \bar{b}_5\dot{x}' + \bar{b}_4\dot{y}' + \bar{b}_6\dot{z}' - \bar{b}_8x' + \bar{b}_{10}y' + \bar{b}_{11}z' + \bar{b}_{13}\frac{\partial\Omega}{\partial y'} \\ \ddot{z}' = \bar{b}_3 - \bar{b}_6\dot{y}' + \bar{b}_4\dot{z}' + \bar{b}_9x' - \bar{b}_{11}y' + \bar{b}_{12}z' + \bar{b}_{13}\frac{\partial\Omega}{\partial z'} \end{cases} \tag{24}$$

Since the Earth–Moon–Sun three body problem was taken to be coplanar, $\bar{b}_3 = \bar{b}_6 = \bar{b}_9 = \bar{b}_{11} = 0, \bar{b}_8 = -\bar{b}_{10}$ in the above equation. The amplitudes of the dynamical substitutes he obtained are close to our results (see Fig. 2.2 $\sim$ 2.4 in that paper). However, the author does not consider the effects of the Moon's orbit eccentricity and inclination. The dynamical substitutes obtained in the thesis is periodic, with the basic frequency ω_3.

In Gómez et al. (2002), this problem was also studied. The motion equations they deduced are of the following form

$$\begin{cases} \ddot{x}' = b_1 + b_4\dot{x}' + b_5\dot{y}' + b_7x' + b_8y' + b_9z' + b_{13}\frac{\partial\Omega}{\partial x'} \\ \ddot{y}' = b_2 - b_5\dot{x}' + b_4\dot{y}' + b_6\dot{z}' - b_8x' + b_{10}y' + b_{11}z' + b_{13}\frac{\partial\Omega}{\partial y'} \\ \ddot{z}' = b_3 - b_6\dot{y}' + b_4\dot{z}' + b_9x' - b_{11}y' + b_{12}z' + b_{13}\frac{\partial\Omega}{\partial z'} \end{cases} \tag{25}$$

in which $b_i, i = 1 \sim 13$ are quasi-periodic functions with the basic frequency set W. They only kept the terms with the basic frequency ω_3 (denoted as ω_2 in that paper) in b_i and called this system as $SSSM_1$. However, the amplitudes of the dynamical substitutes they obtained in this system are much larger than those in Andreu (1998). Since Eq. (24) is the same as Eq. (25) and the methods to compute the dynamical substitutes are the same in both papers, if the computations are correct in Gómez et al. (2002), we speculate the difference is caused by the coefficients in the motion equations. The coefficients in Andreu (1998) are computed by solving the three body problem of the Earth, the Moon and the Sun directly and assuming the Moon's orbit eccentricity and inclination (with respect to the ecliptic) equaling zero. The coefficients in Gómez et al. (2002) are obtained by Fourier analysis. Denote the Moon's orbit eccentricity as e and orbit inclination as i. Due to the property of the Moon's motion (Brouwer and Clemence 1961), following relation holds

$$b_i = \bar{b}_i + \sum_{m,n\geq 0} b_i^{mn} e^m I^n, \tag{26}$$

where $I = \sin(i/2)$, and m, n are even numbers. Considering the fact that $e \sim 0.0549$ and $I \sim 0.0449$ (Murray and Dermott 1999), the difference between b_i and $\bar{b}_i$ can not be neglected.

Another reason that causes the difference in b_i and $\bar{b}_i$ is that the coordinates in Gómez et al. (2002) are rescaled by the instantaneous distances between the Earth and the Moon while the coordinates in Andreu (1998) are not.

4 Linearized motions around the dynamical equivalent

Denote the dynamical substitute as $\bar{X} = (\bar{\xi}, \bar{\eta}, \bar{\zeta}, \dot{\bar{\xi}}, \dot{\bar{\eta}}, \dot{\bar{\zeta}})^T$ and the deviation from it as $\Delta X = X - \bar{X} = (\Delta\xi, \Delta\eta, \Delta\zeta, \Delta\dot{\xi}, \Delta\dot{\eta}, \Delta\dot{\zeta})^T$. In the following discussions, we still denote ΔX as $(\xi, \eta, \zeta, \dot{\xi}, \dot{\eta}, \dot{\zeta})^T$ for brevity. It follows

$$\Delta\dot{X} = A\Delta X + O(\Delta X^2), \quad A = \begin{pmatrix} 0 & I_3 \\ \partial\mathbf{F}_1/\partial\boldsymbol{\rho} & \partial\mathbf{F}_1/\partial\dot{\boldsymbol{\rho}} \end{pmatrix}, \tag{27}$$

where I_3 is an identity matrix. The matrix A is quasi-periodic, with the same basic frequency set W. The transformation $\Delta X = BY$ changes the linear form of Eq. (27) to

$$\dot{Y} = B^{-1}(AB - \dot{B})Y = DY. \tag{28}$$

According to the quasi-Floquet theory (Jorba and Simó 1996), the matrix D can be made constant if B is carefully chosen. Such a transformation matrix B is quasi-periodic, with the same basic frequency set W. Then Eq. (28) can be solved and the linearized solution of Eq. (27) can be obtained by the transformation $\Delta X = BY$. Usually, the matrix B can be obtained approximately with an inductive algorithm (Jorba et al. 1997). The formal step is to find the matrix B to reduce Eq. (27) to the form of Eq. (28) and then obtain the linear solution ΔX. Nevertheless, a different approach is taken in this paper. We first analyze the linearized motion ΔX with the aid of FFT analysis, and then obtain the matrix B. The details will be described below.

Since we are dealing with a Hamiltonian system, the two central components and the maximum Lyapunov exponent indicate that the eigenvalues of the linearized system should be of the form $\pm i v_1, \pm i v_2, \pm v_3$ (Arnold 1999). This suggests us to write Y as

$$Y = (\gamma_1 \cos\theta_1, \quad \gamma_1 \sin\theta_1, \quad \gamma_2 \cos\theta_2, \quad \gamma_2 \sin\theta_2, \quad \gamma_3 e^{v_3 t}, \quad \gamma_4 e^{-v_3 t})^T, \tag{29}$$

where $\theta_1 = v_1 t + \theta_{10}$ and $\theta_2 = v_2 t + \theta_{20}$. θ_{10}, θ_{20} are initial phase angles that can be arbitrarily chosen. The linearized central manifolds are expressed by Eq. (30). The linearized unstable and stable manifolds are expressed by Eq. (31).

$$\begin{cases} \xi_c = b_{11}\gamma_1 \cos\theta_1 + b_{12}\gamma_1 \sin\theta_1 + b_{13}\gamma_2 \cos\theta_2 + b_{14}\gamma_2 \sin\theta_2 \\ \eta_c = b_{21}\gamma_1 \cos\theta_1 + b_{22}\gamma_1 \sin\theta_1 + b_{23}\gamma_2 \cos\theta_2 + b_{24}\gamma_2 \sin\theta_2 \\ \zeta_c = b_{31}\gamma_1 \cos\theta_1 + b_{32}\gamma_1 \sin\theta_1 + b_{33}\gamma_2 \cos\theta_2 + b_{34}\gamma_2 \sin\theta_2 \\ \dot{\xi}_c = b_{41}\gamma_1 \cos\theta_1 + b_{42}\gamma_1 \sin\theta_1 + b_{43}\gamma_2 \cos\theta_2 + b_{44}\gamma_2 \sin\theta_2 \\ \dot{\eta}_c = b_{51}\gamma_1 \cos\theta_1 + b_{52}\gamma_1 \sin\theta_1 + b_{53}\gamma_2 \cos\theta_2 + b_{54}\gamma_2 \sin\theta_2 \\ \dot{\zeta}_c = b_{61}\gamma_1 \cos\theta_1 + b_{62}\gamma_1 \sin\theta_1 + b_{63}\gamma_2 \cos\theta_2 + b_{64}\gamma_2 \sin\theta_2 \end{cases}, \tag{30}$$

$$\begin{cases} \xi_u = b_{15}\gamma_3 e^{v_3 t}, & \eta_u = b_{25}\gamma_3 e^{v_3 t}, & \zeta_u = b_{35}\gamma_3 e^{v_3 t} \\ \dot{\xi}_u = b_{45}\gamma_3 e^{v_3 t}, & \dot{\eta}_u = b_{55}\gamma_3 e^{v_3 t}, & \dot{\zeta}_u = b_{65}\gamma_3 e^{v_3 t} \\ \xi_s = b_{16}\gamma_4 e^{-v_3 t}, & \eta_s = b_{26}\gamma_4 e^{-v_3 t}, & \zeta_s = b_{36}\gamma_4 e^{-v_3 t} \\ \dot{\xi}_s = b_{46}\gamma_4 e^{-v_3 t}, & \dot{\eta}_s = b_{56}\gamma_4 e^{-v_3 t}, & \dot{\zeta}_s = b_{66}\gamma_4 e^{-v_3 t} \end{cases}, \tag{31}$$

where γ_1, γ_2 are amplitudes of the two central components and γ_3, γ_4 are amplitudes of the unstable and stable components. b_{mn} are elements of the matrix B. They are of the form

$$b_{mn} = \sum_{ijkl} C_{mn}^{ijkl} \cos\theta + S_{mn}^{ijkl} \sin\theta, \quad \theta = (i\omega_3 + j\omega_1 + k\omega_2 + l\omega_4)t, \quad 1 \le m, n \le 6. \tag{32}$$

Generally, b_{mn} contains an infinite number of terms. However, truncation to some finite order is necessary and usually enough for some practical uses. Due to the quasi-periodicity, FFT method can be used to analyze b_{mn}. We don't have to compute all the elements in the matrix B. Only the elements $b_{mn}, 1 \le m \le 3, 1 \le n \le 6$ should be computed. Denote the matrix B as $B = (B_1^T, B_2^T)^T$. It can be easily proved that $B_2 = \dot{B}_1 + B_1 D$.

The elements in Eq. (30) can be computed in the following way. First, we construct a quasi-periodic orbit around the dynamical substitute. Then FFT analysis is applied to this orbit. Following are some computational details.

(1) Firstly, we obtain the coefficients $C_{11}^{0000}, C_{12}^{0000}, C_{21}^{0000}, C_{22}^{0000}, C_{31}^{0000}, C_{32}^{0000}$. For the ξ component, denote the coefficients of the frequency v_1 by FFT analysis as $\xi_c^{000010}, \xi_s^{000010}$. Substituting Eq. (32) into the first two equations of Eq. (30), we have

$$\begin{cases} C_{11}^{0000}\gamma_1 \cos\theta_{10} + C_{12}^{0000}\gamma_1 \sin\theta_{10} = \xi_c^{000010} \\ -C_{11}^{0000}\gamma_1 \sin\theta_{10} + C_{12}^{0000}\gamma_1 \cos\theta_{10} = \xi_s^{000010} \end{cases}. \tag{33}$$

In order to solve the above equation, we set $C_{12}^{0000} \equiv 0$ and $C_{11}^{0000} \equiv 1$. Then we obtain the amplitude γ_1 and the initial phase angle θ_{10}.

$$\begin{cases} \gamma_1 = \sqrt{\left(\xi_c^{000010}\right)^2 + \left(\xi_s^{000010}\right)^2} \\ \theta_{10} = \cos^{-1}\left(\xi_c^{000010}/\gamma_1\right) \end{cases}. \tag{34}$$

For the η component, denote the coefficients of the frequency v_1 by FFT analysis as $\eta_c^{000010}, \eta_s^{000010}$. Using the results above, we have

$$\begin{cases} C_{21}^{0000} = \left(\eta_c^{000010}\cos\theta_{10} - \eta_s^{000010}\sin\theta_{10}\right)/\gamma_1 \\ C_{22}^{0000} = \left(\eta_c^{000010}\sin\theta_{10} + \eta_s^{000010}\cos\theta_{10}\right)/\gamma_1 \end{cases}. \tag{35}$$

For the ζ component, similar equations as Eq. (35) can be obtained. In our studies, we find $\zeta_c^{000010} = \zeta_s^{000010} = 0$, thus $C_{31}^{0000} = C_{32}^{0000} = 0$.

(2) Secondly, we solve the coefficients $C_{13}^{0000}, C_{14}^{0000}, C_{23}^{0000}, C_{24}^{0000}, C_{33}^{0000}, C_{34}^{0000}$. For the ζ component, denote the coefficients of the frequency v_2 by FFT analysis as $\zeta_c^{000001}, \zeta_s^{000001}$. Substituting Eq. (32) into the third and the fourth equations in Eq. (30), we have

$$\begin{cases} C_{33}^{0000}\gamma_2 \cos\theta_{20} + C_{34}^{0000}\gamma_2 \sin\theta_{20} = \zeta_c^{000001} \\ -C_{33}^{0000}\gamma_2 \sin\theta_{20} + C_{34}^{0000}\gamma_2 \cos\theta_{20} = \zeta_s^{000001} \end{cases}. \tag{36}$$

Similarly, in order to solve the above equation, we set $C_{34}^{0000} \equiv 0$ and $C_{33}^{0000} \equiv 1$. Then we obtain the amplitude γ_2 and the initial phase angle θ_{20}.

$$\begin{cases} \gamma_2 = \sqrt{\left(\zeta_c^{000001}\right)^2 + \left(\zeta_s^{000001}\right)^2} \\ \theta_{20} = \cos^{-1}\left(\zeta_c^{000001}/\gamma_2\right) \end{cases}. \tag{37}$$

For the ξ, η components, we have

$$\begin{cases} C_{13}^{0000} = \left(\xi_c^{000001}\cos\theta_{20} - \xi_s^{000001}\sin\theta_{20}\right)/\gamma_2 \\ C_{14}^{0000} = \left(\xi_c^{000001}\sin\theta_{20} + \xi_s^{000001}\cos\theta_{20}\right)/\gamma_2 \end{cases}. \tag{38}$$

$$\begin{cases} C_{23}^{0000} = \left(\eta_c^{000001}\cos\theta_{20} - \eta_s^{000001}\sin\theta_{20}\right)/\gamma_2 \\ C_{24}^{0000} = \left(\eta_c^{000001}\sin\theta_{20} + \eta_s^{000001}\cos\theta_{20}\right)/\gamma_2 \end{cases}. \tag{39}$$

In our studies, we find $\xi_c^{000001} = \xi_s^{000001} = 0$ and $\eta_c^{000001} = \eta_s^{000001} = 0$, thus $C_{13}^{0000} = C_{14}^{0000} = 0$ and $C_{23}^{0000} = C_{24}^{0000} = 0$.

(3) Thirdly, we obtain the coefficients $C_{11}^{ijkl}, C_{12}^{ijkl}, C_{21}^{ijkl}, C_{22}^{ijkl}, C_{31}^{ijkl}, C_{32}^{ijkl}$. Taking ξ component as an example. Denote the coefficients of the frequency $(i\omega_3 + j\omega_1 + k\omega_2 + l\omega_4 - v_1)$ as $\xi_c^{ijkl-10}, \xi_s^{ijkl-10}$ and the coefficients of the frequency $(i\omega_3 + j\omega_1 + k\omega_2 + l\omega_4 + v_1)$

as ξ_c^{ijkl10}, ξ_s^{ijkl10}. Substituting Eq. (32) into the first two equations of Eq. (30), we have

$$\begin{aligned}
&\gamma_1 C_{11}^{ijkl}\cos\theta\cos(v_1t+\theta_{10})+\gamma_1 S_{11}^{ijkl}\sin\theta\cos(v_1t+\theta_{10})\\
&\quad+\gamma_1 C_{12}^{ijkl}\cos\theta\sin(v_1t+\theta_{10})+\gamma_1 S_{12}^{ijkl}\sin\theta\sin(v_1t+\theta_{10})\\
&=\xi_c^{ijkl-10}\cos(\theta-v_1t)+\xi_s^{ijkl-10}\sin(\theta-v_1t)\\
&\quad+\xi_c^{ijkl10}\cos(\theta+v_1t)+\xi_s^{ijkl10}\sin(\theta+v_1t)
\end{aligned}\tag{40}$$

Equation (40) can be separated into

$$\begin{cases}
\frac{1}{2}\cos\theta_{10}C_{11}^{ijkl}-\frac{1}{2}\sin\theta_{10}S_{11}^{ijkl}+\frac{1}{2}\sin\theta_{10}C_{12}^{ijkl}+\frac{1}{2}\cos\theta_{10}S_{12}^{ijkl}=\xi_c^{ijkl-10}/\gamma_1\\
-\frac{1}{2}\sin\theta_{10}C_{11}^{ijkl}-\frac{1}{2}\cos\theta_{10}S_{11}^{ijkl}+\frac{1}{2}\cos\theta_{10}C_{12}^{ijkl}-\frac{1}{2}\sin\theta_{10}S_{12}^{ijkl}=\xi_s^{ijkl-10}/\gamma_1\\
\frac{1}{2}\cos\theta_{10}C_{11}^{ijkl}+\frac{1}{2}\sin\theta_{10}S_{11}^{ijkl}+\frac{1}{2}\sin\theta_{10}C_{12}^{ijkl}-\frac{1}{2}\cos\theta_{10}S_{12}^{ijkl}=\xi_c^{ijkl10}/\gamma_1\\
-\frac{1}{2}\sin\theta_{10}C_{11}^{ijkl}+\frac{1}{2}\cos\theta_{10}S_{11}^{ijkl}+\frac{1}{2}\cos\theta_{10}C_{12}^{ijkl}+\frac{1}{2}\sin\theta_{10}S_{12}^{ijkl}=\xi_s^{ijkl10}/\gamma_1
\end{cases}.\tag{41}$$

The solution is

$$\begin{cases}
C_{11}^{ijkl}=\left[\cos\theta_{10}\left(\xi_c^{ijkl10}+\xi_c^{ijkl-10}\right)-\sin\theta_{10}\left(\xi_s^{ijkl10}+\xi_s^{ijkl-10}\right)\right]/\gamma_1\\
S_{11}^{ijkl}=\left[\sin\theta_{10}\left(\xi_c^{ijkl10}-\xi_c^{ijkl-10}\right)+\cos\theta_{10}\left(\xi_s^{ijkl10}-\xi_s^{ijkl-10}\right)\right]/\gamma_1\\
C_{12}^{ijkl}=\left[\sin\theta_{10}\left(\xi_c^{ijkl10}+\xi_c^{ijkl-10}\right)+\cos\theta_{10}\left(\xi_s^{ijkl10}+\xi_s^{ijkl-10}\right)\right]/\gamma_1\\
S_{12}^{ijkl}=\left[-\cos\theta_{10}\left(\xi_c^{ijkl10}-\xi_c^{ijkl-10}\right)+\sin\theta_{10}\left(\xi_s^{ijkl10}-\xi_s^{ijkl-10}\right)\right]/\gamma_1
\end{cases}.\tag{42}$$

C_{21}^{ijkl}, S_{21}^{ijkl}, C_{22}^{ijkl}, S_{22}^{ijkl}, C_{31}^{ijkl}, S_{31}^{ijkl}, C_{32}^{ijkl}, S_{32}^{ijkl} can be computed in the same way.

(4) At last, we obtain the coefficients C_{13}^{ijkl}, C_{14}^{ijkl}, C_{23}^{ijkl}, C_{24}^{ijkl}, C_{33}^{ijkl}, C_{34}^{ijkl}. Also taking ξ component as an example. Denote the coefficients of the frequency $(i\omega_3+j\omega_1+k\omega_2+l\omega_4-v_2)$ as $\xi_c^{ijkl0-1}$, $\xi_s^{ijkl0-1}$ and the coefficients of the frequency $(i\omega_3+j\omega_1+k\omega_2+l\omega_4+v_2)$ as ξ_c^{ijkl01}, ξ_s^{ijkl01}. Similar to step (3), we have

$$\begin{cases}
C_{13}^{ijkl}=\left[\cos\theta_{20}\left(\xi_c^{ijkl01}+\xi_c^{ijkl0-1}\right)-\sin\theta_{20}\left(\xi_s^{ijkl01}+\xi_s^{ijkl0-1}\right)\right]/\gamma_2\\
S_{13}^{ijkl}=\left[\sin\theta_{20}\left(\xi_c^{ijkl01}-\xi_c^{ijkl0-1}\right)+\cos\theta_{20}\left(\xi_s^{ijkl01}-\xi_s^{ijkl0-1}\right)\right]/\gamma_2\\
C_{14}^{ijkl}=\left[\sin\theta_{20}\left(\xi_c^{ijkl01}+\xi_c^{ijkl0-1}\right)+\cos\theta_{20}\left(\xi_s^{ijkl01}+\xi_s^{ijkl0-1}\right)\right]/\gamma_2\\
S_{14}^{ijkl}=\left[-\cos\theta_{20}\left(\xi_c^{ijkl01}-\xi_c^{ijkl0-1}\right)+\sin\theta_{20}\left(\xi_s^{ijkl01}-\xi_s^{ijkl0-1}\right)\right]/\gamma_2
\end{cases}.\tag{43}$$

C_{23}^{ijkl}, S_{23}^{ijkl}, C_{24}^{ijkl}, S_{24}^{ijkl}, C_{33}^{ijkl}, S_{33}^{ijkl}, C_{34}^{ijkl}, S_{34}^{ijkl} can be computed in the same way.

A little bit should be said about the way to construct the quasi-periodic orbit. In the computation of the dynamical substitutes in Sect. 3, we've already obtained quasi-periodic orbits which are very close to the dynamical substitutes. The amplitudes of the central manifolds of these quasi-periodic orbits are very small. We cannot compute all the C_{mn}^{ijkl}, S_{mn}^{ijkl} from these orbits. However, the primary terms of the central manifolds, i.e., the C_{11}^{0000}, C_{12}^{0000}, C_{21}^{0000}, C_{22}^{0000} and C_{33}^{0000}, S_{33}^{0000} can be obtained. Using them as a coarse approximation of the central manifolds, quasi-periodic orbits with central manifolds of larger amplitude can be obtained. On the other hand, the central manifolds can't be too large to avoid the nonlinear terms in the central manifolds. The orbits used in our work are of the order $\gamma_1, \gamma_2 \sim 10^{-4}$, and we only consider periodic terms in b_{mn} with amplitudes till the order 10^{-4}.

The elements b_{mn} in Eq. (31) can be computed in the following way. Take the unstable component as an example. If the initial deviation ΔX_0 is on the unstable direction, then $\Delta X(t)/e^{v_3 t}$ produces the elements $\gamma_3 b_{i5}(t), i = 1, \ldots, 6$. In order to keep the integrated orbit within the proximity of the dynamical substitute, we reset the initial condition of the integrated orbit every after a fixed time Δt as we did in Fig. 6. The norm of the initial deviation in our computations is $d_0 = 10^{-6}$. The interval of the sampling data $\Delta t'$ can be taken as $\Delta t' = \Delta t/N$, where N is an integer. This means N sampling data will be taken in every integrated orbit segment. In our work, $N = 8$. Take the ξ component as an example. In every integrated orbit segment, the sampling data are denoted as

$$\mathtt{sig}(t_{i\times N+j}) = \frac{\xi_u(t_{i\times N+j})}{\xi_u(t_{i\times N})e^{v_3 j\Delta t'}} = \frac{b_{15}(t_{i\times N+j})}{b_{15}(t_{i\times N})}, \quad 1 \le j \le N, \quad i \ge 0. \tag{44}$$

After all the sampling data are obtained, they are improved by the following formula to obtain the signals of b_{15}.

$$b_{15}(t_{i\times N+j}) = \mathtt{sig}(t_{i\times N+j}) \cdot b_{15}(t_{i\times N}), \quad 1 \le j \le N, \quad i \ge 0. \tag{45}$$

Following are the details. Denote the initial deviation of the first orbit segment at the time t_0 as $\mathbf{d}_0 = (d_0^1, d_0^2, d_0^3, d_0^4, d_0^5, d_0^6)^T$. We take $\gamma_3 b_{15}(t_0) = d_0^1$. For the first orbit segment, we have

$$\gamma_3 b_{15}(t_k) = \mathtt{sig}(t_k) \cdot \gamma_3 b_{15}(t_0), \quad 1 \le k \le 8. \tag{46}$$

The last value $\gamma_3 b_{15}(t_8)$ of the first orbit segment is used to generate the data on the second orbit segment

$$\gamma_3 b_{15}(t_k) = \mathtt{sig}(t_k) \cdot \gamma_3 b_{15}(t_8), \quad 9 \le k \le 16. \tag{47}$$

Similar process goes on until we get all the $\gamma_3 b(t_k)$. These signals are analyzed by FFT method. Denote the series of $\gamma_3 b_{15}(t)$ after FFT analysis as

$$\bar{b}_{15} = \sum_{ijkl} \bar{C}_{15}^{ijkl} \cos\theta + \bar{S}_{15}^{ijkl} \sin\theta, \quad \theta = (i\omega_3 + j\omega_1 + k\omega_2 + l\omega_4)t. \tag{48}$$

If we set C_{15}^{0000} in b_{15} as 1, then $\gamma_3 = \bar{C}_{15}^{0000}$ and $C_{15}^{ijkl} = \bar{C}_{15}^{ijkl}/\gamma_3$, $S_{15}^{ijkl} = \bar{S}_{15}^{ijkl}/\gamma_3$. The same method can be used to analyze the elements $b_{25} \sim b_{65}$. The elements $b_{16} \sim b_{66}$ in the stable manifold can also be computed with this method, by integrating the orbits backwards.

Before we start, we need to know the unstable direction at the starting point of the dynamical substitute and the stable direction at the ending point of the dynamical substitute. In order to obtain these two directions, the length of the constructed dynamical substitute is actually longer than 624 years, from MJD = 16757.4774 to 314311.7538. We choose MJD = 51544.5000 as the starting point and MJD = 279524.7312 as the ending point of the three dynamical substitutes shown in Figs. 2, 3 and 4. We know that for an orbit with unstable and stable manifolds, except for some special directions, deviations at arbitrary directions converge to the unstable direction when integrating forwards and to the stable direction when integrating backwards. The orbit segment from MJD = 16757.4774 to 51544.5000 is used to generate the unstable direction at the starting point (MJD = 51544.5000), and the orbit segment from MJD = 279524.7312 to 314311.7538 is used to generate the stable direction at the ending point (MJD = 279524.7312). The method to compute these directions is the same as Fig. 6, with the same ΔX_0 and Δt. Due to the finite length of the two orbit segments, the obtained directions are just approximate unstable or stable directions, but this is enough for our accuracy requirements (to the magnitude 10^{-4}).

Table 3 One primary periodic term for each element b_{mn}, for L_1

Component	ω_1	ω_2	ω_3	ω_4	c_{mn}^{ijkl}	s_{mn}^{ijkl}	Component	ω_1	ω_2	ω_3	ω_4	c_{mn}^{ijkl}	s_{mn}^{ijkl}
b_{11}	1	0	0	0	0.0094	0.0094	b_{24}	−1	0	0	1	0.0011	−0.0013
b_{12}	1	0	0	0	−0.1451	0.1446	b_{25}	1	0	0	0	−0.0769	0.0704
b_{13}	−1	0	0	1	−0.0003	0.0004	b_{26}	1	0	0	0	−0.0706	0.0767
b_{14}	−1	0	0	1	0.0001	0.0001	b_{31}	−1	0	0	1	0.0039	−0.0044
b_{15}	1	0	0	0	0.1831	−0.1274	b_{32}	−1	0	0	1	0.0012	0.0011
b_{16}	1	0	0	0	−0.1280	0.1826	b_{33}	1	0	0	0	0.0310	0.0311
b_{21}	1	0	0	0	−0.5282	0.5265	b_{34}	1	0	0	0	−0.1400	0.1396
b_{22}	1	0	0	0	−0.1028	−0.1031	b_{35}	0	0	0	1	−0.0001	−0.0001
b_{23}	−1	0	0	1	0.0004	0.0003	b_{36}	0	0	0	1	−0.0001	0.0001

The form of Y suggests us that the matrix D in Eq. (28) should be of the form

$$D = \begin{pmatrix} 0 & -v_1 & 0 & 0 & 0 & 0 \\ v_1 & 0 & 0 & 0 & 0 & 0 \\ 0 & 0 & 0 & -v_2 & 0 & 0 \\ 0 & 0 & v_2 & 0 & 0 & 0 \\ 0 & 0 & 0 & 0 & v_3 & 0 \\ 0 & 0 & 0 & 0 & 0 & -v_3 \end{pmatrix}. \tag{49}$$

Since we only collect periodic terms till the order 10^{-4} in the elements b_{mn}, the actually computed matrix $D' = B^{-1}(AB - \dot{B})$ does not exactly have a form of Eq. (49). The biggest periodic term in $D' - \bar{D}'$ is of the magnitude 2×10^{-4}, where the matrix $\bar{D}'$ is defined in Eq. (50) (for the point L_1) and Eq. (51) (for the point L_2). Accurate to 10^{-4}, the matrix $\bar{D}'$ does have a form of Eq. (49).

$$\bar{D}' = \lim_{T\to\infty} \frac{1}{T} \int_0^T D' \cdot \mathrm{d}t \approx \begin{pmatrix} 0 & -2.3377 & 0 & 0 & 0 & 0 \\ 2.3377 & 0 & 0 & 0 & 0 & 0 \\ 0 & 0 & 0 & -2.2743 & 0 & 0 \\ 0 & 0 & 2.2743 & 0 & 0 & 0 \\ 0 & 0 & 0 & 0 & 2.9392 & 0 \\ 0 & 0 & 0 & 0 & 0 & -2.9392 \end{pmatrix}, \tag{50}$$

$$\bar{D}' = \lim_{T\to\infty} \frac{1}{T} \int_0^T D' \cdot \mathrm{d}t \approx \begin{pmatrix} 0 & -1.8646 & 0 & 0 & 0 & 0 \\ 1.8646 & 0 & 0 & 0 & 0 & 0 \\ 0 & 0 & 0 & -1.7909 & 0 & 0 \\ 0 & 0 & 1.7909 & 0 & 0 & 0 \\ 0 & 0 & 0 & 0 & 2.1648 & 0 \\ 0 & 0 & 0 & 0 & 0 & -2.1648 \end{pmatrix}. \tag{51}$$

In order to check the results, Table 3 (for the point L_1) and Table 4 (for the point L_2) show one primary periodic term for each element b_{mn}.

Figure 8 shows the deviation between the numerically integrated orbit (solid line) and the linearized analytic solution (dashed line). The initial condition of the integrated orbit is the same as the analytic solution. The starting epoch is MJD = 51553.1967. The two components of the central manifolds γ_1, γ_2 are both taken to be 1×10^{-4} dimensionless units. The initial

Table 4 One primary periodic term for each element b_{mn}, for L_2

Component	ω_1	ω_2	ω_3	ω_4	c_{mn}^{ijkl}	s_{mn}^{ijkl}	Component	ω_1	ω_2	ω_3	ω_4	c_{mn}^{ijkl}	s_{mn}^{ijkl}
b_{11}	1	0	0	0	0.0084	0.0084	b_{24}	−1	0	0	1	0.0011	−0.0012
b_{12}	1	0	0	0	−0.1193	0.1189	b_{25}	1	0	0	0	−0.0750	0.0673
b_{13}	−1	0	0	1	−0.0004	0.0004	b_{26}	1	0	0	0	−0.0675	0.0747
b_{14}	−1	0	0	1	0.0001	0.0001	b_{31}	−1	0	0	1	0.0027	−0.0030
b_{15}	1	0	0	0	0.1340	−0.0773	b_{32}	−1	0	0	1	0.0008	0.0007
b_{16}	1	0	0	0	−0.0777	0.1337	b_{33}	1	0	0	0	0.0317	0.0318
b_{21}	1	0	0	0	−0.3551	0.3540	b_{34}	1	0	0	0	−0.1135	0.1131
b_{22}	1	0	0	0	−0.0811	−0.0813	b_{35}	0	0	0	1	−0.0002	−0.0001
b_{23}	−1	0	0	1	0.0004	0.0003	b_{36}	0	0	0	1	−0.0002	0.0001

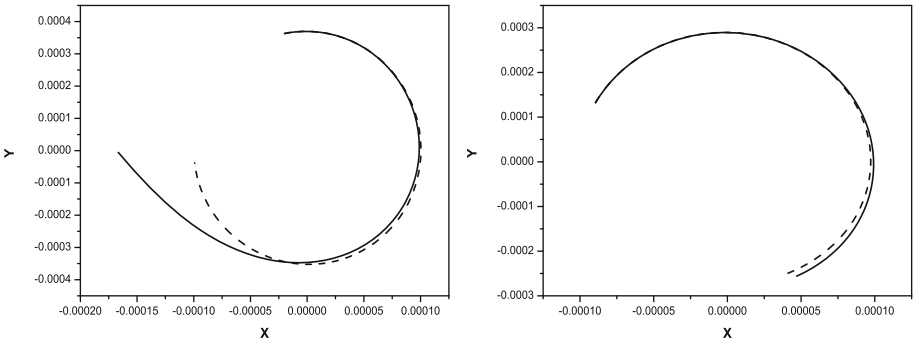

Fig. 8 Deviation between the numerically integrated orbit and the analytic solution given by Eq. (30). The *left frame* is for the point L_1 and the *right frame* is for the point L_2

phase angles θ_{10}, θ_{20} are both 0. The left frame is for the point L_1 and the right frame is for the point L_2. To save space, only projections on the $x - y$ plane are shown.

In the circular restricted three-body problem of the Earth–Moon system, linearized central manifolds around the collinear libration points are expressed as (Jorba and Masdemont 1999)

$$\begin{cases} x = \gamma_1 \cos\left(v_1 t' + \theta_{10}\right) \\ y = \kappa\gamma_1 \sin\left(v_1 t' + \theta_{10}\right) \\ z = \gamma_2 \cos\left(v_2 t' + \theta_{20}\right) \end{cases}, \tag{52}$$

where

$$\begin{cases} C_0 = \frac{\mu_3}{r_0^3} + \frac{\mu_{10}}{\left(\delta_{10}^0\right)^3} \\ v_1' = \sqrt{\frac{\sqrt{9C_0^2 - 8C_0} + 2 - C_0}{2}} \quad v_2' = \sqrt{C_0} \quad \kappa = -\frac{1}{2}\left(v_1' + \frac{(1+2C_0)}{v_1'}\right) \end{cases} \tag{53}$$

For comparison with the linearized central manifolds described by Eq. (30) in the real Earth–Moon system, Fig. 9 gives the integrated orbit with initial conditions given by Eq. (52). The left frame is for L_1 and the right frame is for L_2. The solid lines are the integrated orbit in the real Earth–Moon system and the dashed line are analytic solutions. Obviously, the divergence speed is larger. Compared with Eq. (30), the advantage of the improved linearized solution is obvious, although the solution's form is more complicated.

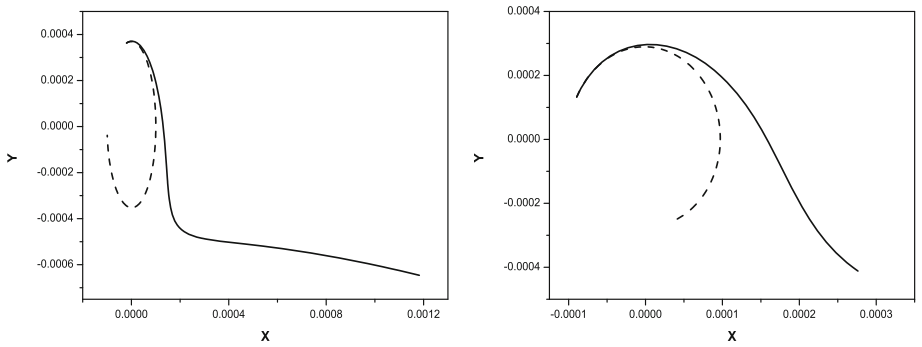

Fig. 9 Deviation between the numerically integrated orbit and the analytic solution given by Eq. (52). The *left frame* is for the point L_1 and the *right frame* is for the point L_2

Using the linearized central manifolds Eq. (30) as initial seeds, quasi-periodic orbits not far away from the dynamical substitute and lasting for quite a long time can be obtained with parallel shooting method. For larger amplitude orbits, Eq. (30) is not accurate enough for the numerical iteration process to converge. Higher order analytical solutions of the central manifolds are needed.

5 High order solutions

Taking the relation $\Delta X = BY$ into Eq. (27), we obtain

$$\dot{Y} - DY = B^{-1}O(\Delta X^2). \tag{54}$$

The literal solution can be constructed by traditional Lindstedt–Poincaré method. Neglecting the very small planetary terms and due to the fact that the amplitude of the dynamical substitutes of the points L_1 and L_2 are very small, $O(\Delta X^2)$ can be approximately taken as the higher order terms of F_1 in Eq. (5).

$$O(\Delta X^2) = \frac{\partial}{\partial \boldsymbol{\rho}} \sum_{n=3}^{\infty} \left\{ \frac{\mu_3}{r_0} \left[\left(\frac{\rho}{r_0} \right)^n P_n \left(\cos \Psi_3' \right) \right] + \frac{\mu_{10}}{\delta_{10}^0} \left[\left(\frac{\rho}{\delta_{10}^0} \right)^n P_n \left(\cos \Psi_{10}' \right) \right] + \frac{\mu_{11}}{\delta_{11}^0} \left[\left(\frac{\rho}{\delta_{11}^0} \right)^n P_n \left(\cos \Psi_{11}' \right) \right] \right\}. \tag{55}$$

The coefficients of the second order terms from the Sun's perturbations are small ($\sim 10^{-5}$). Even if we consider very large amplitude motions ($\Delta X \sim 10^{-1}$), the magnitude of the Sun's high order perturbations is of the magnitude $\sim 10^{-7}$. It's unnecessary to consider these terms due to the fact that the reduction accuracy of the linear terms is only of the magnitude 10^{-4}. As a result, Eq. (55) can be reduced to the form of

$$O(\Delta X^2) = \frac{\partial}{\partial \boldsymbol{\rho}} \sum_{n=3}^{\infty} \left\{ \frac{\mu_3}{r_0} \left[\left(\frac{\rho}{r_0} \right)^n P_n \left(\cos \Psi_3' \right) \right] + \frac{\mu_{10}}{\delta_{10}^0} \left[\left(\frac{\rho}{\delta_{10}^0} \right)^n P_n \left(\cos \Psi_{10}' \right) \right] \right\}. \tag{56}$$

Expanding Eq. (27) as

$$\dot{\Delta X} = A\dot{\Delta X} + (0, 0, 0, F_x, F_y, F_z)^T, \tag{57}$$

where

$$\begin{cases} F_x = \sum\limits_{n\geq 2}^{\infty} c_{n+1}(n+1)T_n\left(\frac{\xi}{\rho}\right) \\ F_y = \eta \sum\limits_{n\geq 2}^{\infty} c_{n+1}R_{n-1}\left(\frac{\xi}{\rho}\right) \\ F_z = \zeta \sum\limits_{n\geq 2}^{\infty} c_{n+1}R_{n-1}\left(\frac{\xi}{\rho}\right) \end{cases}, \tag{58}$$

and

$$\begin{cases} c_n = (-1)^n \frac{\mu_3}{(1+\gamma)^{n+1}r_{10}^{n+1}} + (-1)^{n+1}\frac{\mu_{10}}{\gamma^{n+1}r_{10}^{n+1}}, \quad \text{for} \quad L_1 \\ c_n = (-1)^n \frac{\mu_3}{(1+\gamma)^{n+1}r_{10}^{n+1}} + (-1)^{n}\frac{\mu_{10}}{\gamma^{n+1}r_{10}^{n+1}}, \quad \text{for} \quad L_2 \end{cases}. \tag{59}$$

The functions T_n, R_n are defined as

$$T_n(\xi/\rho) = \rho^n P_n(\xi/\rho), \quad R_{n-1}(\xi/\rho) = \frac{1}{y}\frac{\partial T_{n+1}}{\partial y} = \frac{1}{z}\frac{\partial T_{n+1}}{\partial z}, \tag{60}$$

and the inductive relations below hold (Gómez et al. 2001c).

$$\begin{cases} T_n = \frac{2n-1}{n}\xi T_{n-1} - \frac{n-1}{n}\rho^2 T_{n-2}, \quad T_0 = 1, \quad T_1 = x \\ R_n = \frac{2n+3}{n+2}\xi R_{n-1} - \frac{2n+2}{n+2}T_n - \frac{n+1}{n+2}\rho^2 R_{n-2}, \quad R_0 = -1, \quad R_1 = -3x \end{cases}. \tag{61}$$

5.1 Lissajous orbits

The literal solution of Y can be expressed as

$$\begin{cases} y_1 = \sum\limits_{m',n',i,j,k,l,m,n} \alpha^{m'}\beta^{n'}\left(y_{1c,m'n'}^{ijklmn}\cos\theta + y_{1s,m'n'}^{ijklmn}\sin\theta\right) \\ y_2 = \sum\limits_{m',n',i,j,k,l,m,n} \alpha^{m'}\beta^{n'}\left(y_{2c,m'n'}^{ijklmn}\cos\theta + y_{2s,m'n'}^{ijklmn}\sin\theta\right) \\ y_3 = \sum\limits_{m',n',i,j,k,l,m,n} \alpha^{m'}\beta^{n'}\left(y_{3c,m'n'}^{ijklmn}\cos\theta + y_{3s,m'n'}^{ijklmn}\sin\theta\right) \\ y_4 = \sum\limits_{m',n',i,j,k,l,m,n} \alpha^{m'}\beta^{n'}\left(y_{4c,m'n'}^{ijklmn}\cos\theta + y_{4s,m'n'}^{ijklmn}\sin\theta\right) \\ y_5 = \sum\limits_{m',n',i,j,k,l,m,n} \alpha^{m'}\beta^{n'}\left(y_{5c,m'n'}^{ijklmn}\cos\theta + y_{5s,m'n'}^{ijklmn}\sin\theta\right) \\ y_6 = \sum\limits_{m',n',i,j,k,l,m,n} \alpha^{m'}\beta^{n'}\left(y_{6c,m'n'}^{ijklmn}\cos\theta + y_{6s,m'n'}^{ijklmn}\sin\theta\right) \end{cases}, \tag{62}$$

where α, β are the parameters γ_1, γ_2 in Eq. (30). $\theta = (i\omega_3 + j\omega_1 + k\omega_2 + l\omega_4)t + m\theta_1 + n\theta_2$, and $\theta_1 = v_1 t + \theta_{10}$, $\theta_2 = v_2 t + \theta_{20}$. θ_{10}, θ_{20} are two arbitrarily chosen constants. In the sum, $N = m' + n' \geq 1$ is the order of the solution. m, n should have the same parity as m', n' and satisfy

$$m' \geq 0, \quad n' \geq 0, \quad -m' \leq m \leq m', \quad -n' \leq n \leq n' \tag{63}$$

As stated before, a truncation of i, j, k, l is necessary. In this paper, $0 \le i \le 4, -4 \le j \le 4, -2 \le k \le 2, -2 \le l \le 2$. Similarly, the literal solution of ΔX can also be expressed as

$$\begin{cases} \xi = \sum\limits_{m',n',i,j,k,l,m,n} \alpha^{m'}\beta^{n'}\left(\xi_{c,m'n'}^{ijklmn}\cos\theta + \xi_{s,m'n'}^{ijklmn}\sin\theta\right) \\ \eta = \sum\limits_{m',n',i,j,k,l,m,n} \alpha^{m'}\beta^{n'}\left(\eta_{c,m'n'}^{ijklmn}\cos\theta + \eta_{s,m'n'}^{ijklmn}\sin\theta\right) \\ \zeta = \sum\limits_{m',n',i,j,k,l,m,n} \alpha^{m'}\beta^{n'}\left(\zeta_{c,m'n'}^{ijklmn}\cos\theta + \zeta_{s,m'n'}^{ijklmn}\sin\theta\right) \\ \dot{\xi} = \sum\limits_{m',n',i,j,k,l,m,n} \alpha^{m'}\beta^{n'}\left(\dot{\xi}_{c,m'n'}^{ijklmn}\cos\theta + \dot{\xi}_{s,m'n'}^{ijklmn}\sin\theta\right) \\ \dot{\eta} = \sum\limits_{m',n',i,j,k,l,m,n} \alpha^{m'}\beta^{n'}\left(\dot{\eta}_{c,m'n'}^{ijklmn}\cos\theta + \dot{\eta}_{s,m'n'}^{ijklmn}\sin\theta\right) \\ \dot{\zeta} = \sum\limits_{m',n',i,j,k,l,m,n} \alpha^{m'}\beta^{n'}\left(\dot{\zeta}_{c,m'n'}^{ijklmn}\cos\theta + \dot{\zeta}_{6s,m'n'}^{ijklmn}\sin\theta\right) \end{cases}, \tag{64}$$

The two frequencies v_1 and v_2 should be expanded as

$$v_1 = \sum_{m'n'} v_1^{m'n'}\alpha^{m'}\beta^{n'}, \quad v_2 = \sum_{m'n'} v_2^{m'n'}\alpha^{m'}\beta^{n'} \tag{65}$$

where m', n' should satisfy $m', n' \ge 0$ and should be even numbers.

Suppose Y and ΔX are already solved to the order $N-1$ (The frequencies v_1, v_2 are solved to the order $N-2$). Taking ΔX till order $N-1$ and v_1, v_2 till order $N-2$ into Eq. (54), we obtain the equation of Y of the order N, with the unknown at the left side of the equation and the known at the right side of the equation.

$$\begin{cases} \omega_{ijklmn} y_{1s,m'n'}^{ijklmn} + v_1^{00} y_{2c,m'n'}^{ijklmn} = p_{1c,m'n'}^{ijklmn} \\ -\omega_{ijklmn} y_{1c,m'n'}^{ijklmn} + v_1^{00} y_{2s,m'n'}^{ijklmn} - \delta_1 v_1^{m'-1,n'} = p_{1s,m'n'}^{ijklmn} \\ \omega_{ijklmn} y_{2s,m'n'}^{ijklmn} - v_1^{00} y_{1c,m'n'}^{ijklmn} + \delta_1 v_1^{m'-1,n'} = p_{2c,m'n'}^{ijklmn} \\ -\omega_{ijklmn} y_{2c,m'n'}^{ijklmn} - v_1^{00} y_{1s,m'n'}^{ijklmn} = p_{2s,m'n'}^{ijklmn} \end{cases}, \tag{66}$$

$$\begin{cases} \omega_{ijklmn} y_{3s,m'n'}^{ijklmn} + v_2^{00} y_{4c,m'n'}^{ijklmn} = p_{3c,m'n'}^{ijklmn} \\ -\omega_{ijklmn} y_{3c,m'n'}^{ijklmn} + v_2^{00} y_{4s,m'n'}^{ijklmn} - \delta_2 v_2^{m',n'-1} = p_{3s,m'n'}^{ijklmn} \\ \omega_{ijklmn} y_{4s,m'n'}^{ijklmn} - v_2^{00} y_{3c,m'n'}^{ijklmn} + \delta_2 v_2^{m',n'-1} = p_{4c,m'n'}^{ijklmn} \\ -\omega_{ijklmn} y_{4c,m'n'}^{ijklmn} - v_2^{00} y_{3s,m'n'}^{ijklmn} = p_{4s,m'n'}^{ijklmn} \end{cases}, \tag{67}$$

$$\begin{cases} \omega_{ijklmn} y_{5s,m'n'}^{ijklmn} - v_3 y_{5c,m'n'}^{ijklmn} = p_{5c,m'n'}^{ijklmn} \\ -\omega_{ijklmn} y_{5c,m'n'}^{ijklmn} - v_3 y_{5s,m'n'}^{ijklmn} = p_{5s,m'n'}^{ijklmn} \\ \omega_{ijklmn} y_{6s,m'n'}^{ijklmn} + v_3 y_{6c,m'n'}^{ijklmn} = p_{6c,m'n'}^{ijklmn} \\ -\omega_{ijklmn} y_{6c,m'n'}^{ijklmn} + v_3 y_{6s,m'n'}^{ijklmn} = p_{6s,m'n'}^{ijklmn} \end{cases}, \tag{68}$$

where $p_{*c,m'n'}^{ijklmn}$, $p_{*s,m'n'}^{ijklmn}$ are known terms. $\omega_{ijklmn} = i\omega_3 + j\omega_1 + k\omega_2 + l\omega_4 + mv_1^{00} + nv_2^{00}$. δ_1 equals 1 when $i = j = k = l = n = 0, m = 1$ and equals 0 otherwise. δ_2 equals 1 when $i = j = k = l = m = 0, n = 1$ and equals 0 otherwise. When $\delta_1 = 0$ and $\delta_2 = 0$, we simply solve Eq. (66) $\sim$ (68) to obtain $y_{*c,m'n'}^{ijklmn}$, $y_{*s,m'n'}^{ijklmn}$. When $\delta_1 = 1$, it can be proved that $p_{1c,m'n'}^{000010} = p_{2s,m'n'}^{000010} = 0$ (see the Appendix). As a result, $y_{2c,m'n'}^{000010} = y_{1s,m'n'}^{000010} = 0$. Although the actually computed values of $p_{1c,m'n'}^{000010}$, $p_{2s,m'n'}^{000010}$ do not equal zero due to the fact that we only have approximate linear solutions, they are significantly small compared with

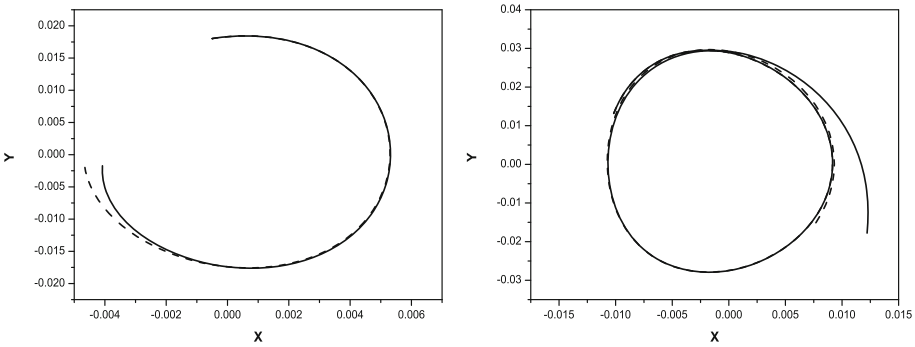

Fig. 10 Deviation between the numerically integrated orbit and the analytic solution Eq. (64). The *left frame* is for the point L_1 and the *right frame* is for the point L_2

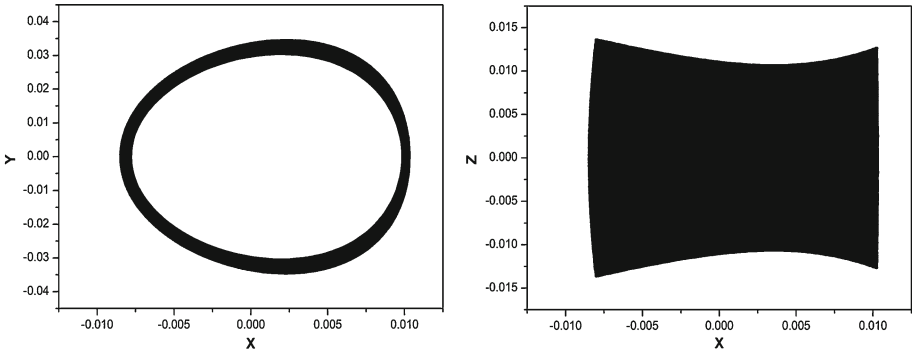

Fig. 11 One Lissajous orbit around the point L_1, lasting 624 years

$p^{000010}_{2c,m'n'}$, $p^{000010}_{1s,m'n'}$. As a result, they are actually taken to be zeros in our construction process. We also set $y^{000010}_{2s,m'n'} = 0$ to solve $y^{000010}_{1c,m'n'}$ and $v_1^{m'-1,n}$ from the second and third equations in Eq. (66). The case of $\delta_2 = 1$ is similar to that of $\delta_1 = 1$. We set $y^{000001}_{3s,m'n'} = y^{000001}_{4c,m'n'} = 0$, and we set $y^{000001}_{4s,m'n'} = 0$ to solve $y^{000001}_{3c,m'n'}$ and $v_2^{m',n-1}$ from the second and third equations in Eq. (67).

Due to the large storage problem, we only construct the analytical solution up to the order five. Figure 10 shows the deviation between the integrated orbit (solid line) and the analytic solution (dashed line). The initial epoch is MJD = 51553.1967. To save space, only projections on the $x - y$ plane are given. The left frame is for the point L_1. The initial conditions are $\gamma_1 = 5 \times 10^{-3}$, $\gamma_2 = 5 \times 10^{-3}$, $\theta_{10} = \theta_{20} = 0$. The right frame is for the point L_2. The initial conditions are $\gamma_1 = 1 \times 10^{-2}$, $\gamma_2 = 1 \times 10^{-2}$, $\theta_{10} = \theta_{20} = 0$

In our work, we find that for large amplitude motions, the deviation speed is larger for analytic solution of order five than that of order three. This means the literal series is divergent for larger amplitude motions. We'll talk about this later at the end of this section.

Using the high order analytic solutions as initial seeds, Lissajous orbits around the points L_1, L_2 can be constructed by the parallel shooting method. For smaller amplitude orbits, the initial seed is accurate enough for the numerical process to converge. For larger amplitude orbits, the convergence speed is not satisfactory if we want to construct a long Lissajous orbit. Figures 11 and 12 show one Lissajous orbit around the point L_1 and L_2 respectively.

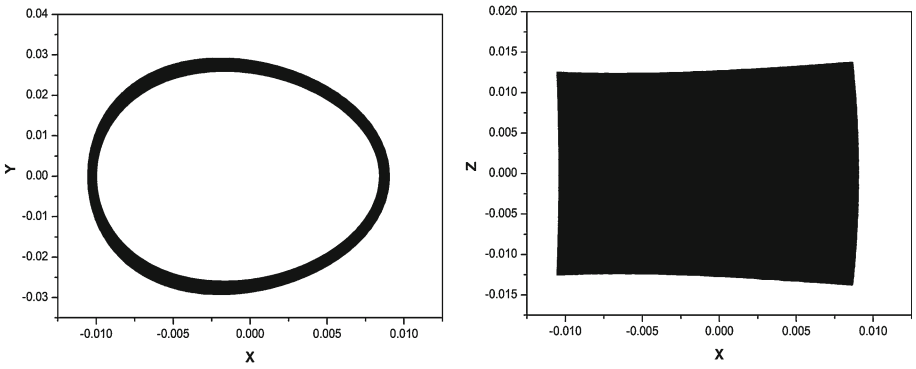

Fig. 12 One Lissajous orbit around the point L_2, lasting 624 years

Table 5 Coefficients in the frequencies v_1, v_2 for the Lissajous orbit

Frequency	v_i^{20}	v_i^{02}	v_i^{40}	v_i^{22}	v_i^{04}
$L_1 - v_1$	−185.2783	−3.7047	1042.0666	25201.1218	−1145.1593
$L_1 - v_2$	−41.5118	−14.7612	141582.6737	−25254.0426	−180.6358
$L_2 - v_1$	−23.6111	2.8571	−2389.9114	3030.8158	−201.4437
$L_2 - v_2$	19.1160	−2.3384	10401.7168	−2773.6950	−42.9067

For both orbits, the amplitudes are $\alpha = 0.0090, \beta = 0.0090$. The orbits constructed last 624 years. The time interval between consecutive nodal points is 0.8 dimensionless units and totally 65537 nodal points are used.

The list of all the primary terms in the solution is too long. To save space, we prefer to only list the coefficients of the frequencies for readers to check the results (see Table 5).

5.2 Halo orbits

For large amplitude motions, it's possible for $v_1 = v_2$ due to the nonlinear terms in Eq. (65). In such a case, only one basic frequency v_1 exists. The solution of Y and ΔX can be expressed as

$$\begin{cases} y_1 = \sum\limits_{m',n',i,j,k,l,m} \alpha^{m'} \beta^{n'} \left(y_{1c,m'n'}^{ijklm} \cos\theta + y_{1s,m'n'}^{ijklm} \sin\theta \right) \\ y_2 = \sum\limits_{m',n',i,j,k,l,m} \alpha^{m'} \beta^{n'} \left(y_{2c,m'n'}^{ijklm} \cos\theta + y_{2s,m'n'}^{ijklm} \sin\theta \right) \\ y_3 = \sum\limits_{m',n',i,j,k,l,m} \alpha^{m'} \beta^{n'} \left(y_{3c,m'n'}^{ijklm} \cos\theta + y_{3s,m'n'}^{ijklm} \sin\theta \right) \\ y_4 = \sum\limits_{m',n',i,j,k,l,m} \alpha^{m'} \beta^{n'} \left(y_{4c,m'n'}^{ijklm} \cos\theta + y_{4s,m'n'}^{ijklm} \sin\theta \right) \\ y_5 = \sum\limits_{m',n',i,j,k,l,m} \alpha^{m'} \beta^{n'} \left(y_{5c,m'n'}^{ijklm} \cos\theta + y_{5s,m'n'}^{ijklm} \sin\theta \right) \\ y_6 = \sum\limits_{m',n',i,j,k,l,m} \alpha^{m'} \beta^{n'} \left(y_{6c,m'n'}^{ijklm} \cos\theta + y_{6s,m'n'}^{ijklm} \sin\theta \right) \end{cases}, \tag{69}$$

$$\begin{cases} \xi = \sum\limits_{m',n',i,j,k,l,m} \alpha^{m'}\beta^{n'}\left(\xi_{c,m'n'}^{ijklm}\cos\theta + \xi_{s,m'n'}^{ijklm}\sin\theta\right) \\ \eta = \sum\limits_{m',n',i,j,k,l,m} \alpha^{m'}\beta^{n'}\left(\eta_{c,m'n'}^{ijklm}\cos\theta + \eta_{s,m'n'}^{ijklm}\sin\theta\right) \\ \zeta = \sum\limits_{m',n',i,j,k,l,m} \alpha^{m'}\beta^{n'}\left(\zeta_{c,m'n'}^{ijklm}\cos\theta + \zeta_{s,m'n'}^{ijklm}\sin\theta\right) \\ \dot{\xi} = \sum\limits_{m',n',i,j,k,l,m} \alpha^{m'}\beta^{n'}\left(\dot{\xi}_{c,m'n'}^{ijklm}\cos\theta + \dot{\xi}_{s,m'n'}^{ijklm}\sin\theta\right) \\ \dot{\eta} = \sum\limits_{m',n',i,j,k,l,m} \alpha^{m'}\beta^{n'}\left(\dot{\eta}_{c,m'n'}^{ijklm}\cos\theta + \dot{\eta}_{s,m'n'}^{ijklm}\sin\theta\right) \\ \dot{\zeta} = \sum\limits_{m',n',i,j,k,l,m} \alpha^{m'}\beta^{n'}\left(\dot{\zeta}_{c,m'n'}^{ijklm}\cos\theta + \dot{\zeta}_{s,m'n'}^{ijklm}\sin\theta\right) \end{cases}, \tag{70}$$

where $\theta = (i\omega_3 + j\omega_1 + k\omega_2 + l\omega_4)t + m\theta_1$, and $\theta_1 = v_1 t + \theta_{10}$. θ_{10} is an arbitrarily chosen constant. In the sum, $N = m' + n' \geq 1$ is the order of the solution. m has the same parity as $m' + n'$ and should satisfy

$$m' \geq 0, \quad n' \geq 0, \quad -m' - n' \leq m \leq m' + n' \tag{71}$$

Similarly, the truncation $0 \leq i \leq 4$, $-4 \leq j \leq 4$, $-2 \leq k \leq 2$, $-2 \leq l \leq 2$ is made.

Rewrite Eq. (54) as

$$\begin{cases} \dot{y_1} + v_1^{00} y_2 = [B^{-1}O(\Delta X^2)]_1 \\ \dot{y_2} - v_1^{00} y_1 = [B^{-1}O(\Delta X^2)]_2 \\ \dot{y_3} + v_1^{00} y_4 = \left(v_1^{00} - v_2^{00}\right) y_4 + [B^{-1}O(\Delta X^2)]_3 \\ \dot{y_4} - v_1^{00} y_3 = -\left(v_1^{00} - v_2^{00}\right) y_3 + [B^{-1}O(\Delta X^2)]_4 \\ \dot{y_5} - v_3 y_5 = [B^{-1}O(\Delta X^2)]_5 \\ \dot{y_6} + v_3 y_6 = [B^{-1}O(\Delta X^2)]_6 \end{cases}, \tag{72}$$

Let

$$v_1 = \sum_{m'n'} v_1^{m'n'}\alpha^{m'}\beta^{n'}, \quad v_1^{00} - v_2^{00} = \sum_{m'n'} d^{m'n'}\alpha^{m'}\beta^{n'} \tag{73}$$

where m', n' should satisfy $m', n' \geq 0$ and should be even numbers. For the second equation in Eq. (73), $m' + n' \geq 2$.

Suppose Y and ΔX are already solved to the order $N-1$ ($v_1^{m'n'}$ and $d^{m'n'}$ are solved to the order $N-2$). Taking ΔX till order $N-1$ and $v_1^{m'n'}$, $d^{m'n'}$ till order $N-2$ into Eq. (72), we obtain the equation of Y of the order N, with the unknown at the left side of the equation and the known at the right side of the equation.

$$\begin{cases} \omega_{ijklm} y_{1s,m'n'}^{ijklm} + v_1^{00} y_{2c,m'n'}^{ijklm} = p_{1c,m'n'}^{ijklm} \\ -\omega_{ijklm} y_{1c,m'n'}^{ijklm} + v_1^{00} y_{2s,m'n'}^{ijklm} - \delta v_1^{m'-1,n'} = p_{1s,m'n'}^{ijklm} \\ \omega_{ijklm} y_{2s,m'n'}^{ijklm} - v_1^{00} y_{1c,m'n'}^{ijklm} + \delta v_1^{m'-1,n'} = p_{2c,m'n'}^{ijklm} \\ -\omega_{ijklm} y_{2c,m'n'}^{ijklm} - v_1^{00} y_{1s,m'n'}^{ijklm} = p_{2s,m'n'}^{ijklm} \end{cases}, \tag{74}$$

$$\begin{cases} \omega_{ijklm} y_{3s,m'n'}^{ijklm} + v_1^{00} y_{4c,m'n'}^{ijklm} = p_{3c,m'n'}^{ijklm} \\ -\omega_{ijklm} y_{3c,m'n'}^{ijklm} + v_1^{00} y_{4s,m'n'}^{ijklm} - \delta v_1^{m',n'-1} - \delta d^{m',n'-1} = p_{3s,m'n'}^{ijklm} \\ \omega_{ijklm} y_{4s,m'n'}^{ijklm} - v_1^{00} y_{3c,m'n'}^{ijklm} + \delta v_1^{m',n'-1} + \delta d^{m',n'-1} = p_{4c,m'n'}^{ijklm} \\ -\omega_{ijklm} y_{4c,m'n'}^{ijklm} - v_1^{00} y_{3s,m'n'}^{ijklm} = p_{4s,m'n'}^{ijklm} \end{cases}, \tag{75}$$

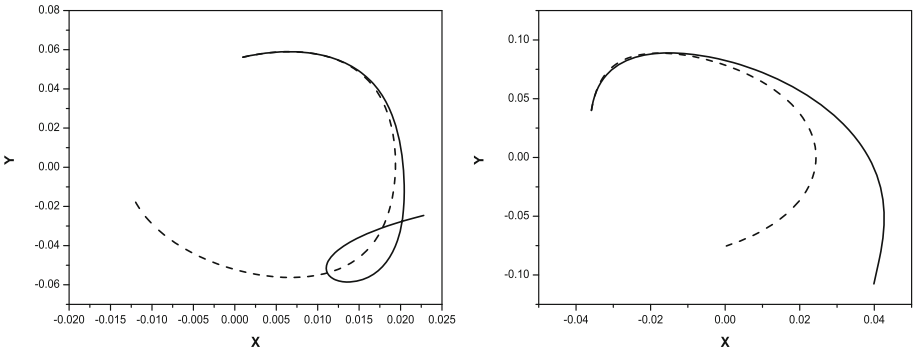

Fig. 13 Deviation between the numerically integrated orbit and the analytic solution provided by Eq. (70) for the point L_1. The *left frame* is the point L_1 and the *right frame* is for the point L_2

$$\begin{cases} \omega_{ijklm} y^{ijklm}_{5s,m'n'} - v_3 y^{ijklm}_{5c,m'n'} = p^{ijklm}_{5c,m'n'} \\ -\omega_{ijklm} y^{ijklm}_{5c,m'n'} - v_3 y^{ijklm}_{5s,m'n'} = p^{ijklm}_{5s,m'n'} \\ \omega_{ijklm} y^{ijklm}_{6s,m'n'} + v_3 y^{ijklm}_{6c,m'n'} = p^{ijklm}_{6c,m'n'} \\ -\omega_{ijklm} y^{ijklm}_{6c,m'n'} + v_3 y^{ijklm}_{6s,m'n'} = p^{ijklm}_{6s,m'n'} \end{cases}, \tag{76}$$

where $p^{ijklm}_{*c,m'n'}$, $p^{ijklm}_{*s,m'n'}$ are known terms. $\omega_{ijklm} = i\omega_3 + j\omega_1 + k\omega_2 + l\omega_4 + mv_1^{00}$. δ equals 1 when $i = j = k = l = 0, m = 1$ and equals 0 otherwise. When $\delta = 0$, we simply solve Eq. (74)∼(76) to obtain $y^{ijklm}_{*c,m'n'}$, $y^{ijklm}_{*s,m'n'}$. When $\delta = 1$, similar to the Lissajous case, $p^{00001}_{1c,m'n'} = p^{00001}_{2s,m'n'} = 0$ and $p^{00001}_{3c,m'n'} = p^{00001}_{4s,m'n'} = 0$. As a result, $y^{00001}_{1s,m'n'} = y^{00001}_{2c,m'n'} = 0$ and $y^{00001}_{3s,m'n'} = y^{00001}_{4c,m'n'} = 0$. We first set $y^{ijklm}_{2s,m'n'} = 0$ to solve $y^{00001}_{1c,m'n'}$ and $v_1^{m'-1,n'}$ from the second and thrid equations in Eq. (74). After we obtain all the coefficients of the order $N-1$ in the frequency v_1, we substitute $v_1^{m',n-1}$ into Eq. (75) and set $y^{ijklm}_{4s,m'n'} = 0$ to solve $y^{00001}_{3c,m'n'} = 0$ and $d^{m',n'-1}$ from the second and thrid equations in Eq. (74).

Also due to the large storage problem, we only construct the analytical solution up to the order seven. Figure 13 shows the deviation between the integrated orbit (solid line) and the analytic solution (dashed line). The initial epoch is MJD = 51553.1967. The initial condition of the integrated orbit is the same as the analytic solution. To save space, only $x - y$ projections are given. The left frame is for the point L_1. $\alpha = 0.0160$, $\beta = 0.0188$, $\theta_{10} = \theta_{20} = 0$. The right frame is for the point L_2. $\alpha = 0.0300$, $\beta = 0.0180$, $\theta_{10} = \theta_{20} = 0$. In fact, due to the divergence problem discussed below, the analytic solutions shown in the frames are of the order three.

Using this analytical solution as the initial seed, halo orbits around the points L_1, L_2 can be constructed by the parallel shooting method. Figures 14 and 15 show one halo orbit around the points L_1 and L_2, respectively. In Fig. 14, the initial conditions are $\alpha = 0.0160$, $\beta = 0.0188$, $\theta_{10} = \theta_{20} = 0$. The orbit constructed lasts 624 years. In Fig. 15, the initial conditions are $\alpha = 0.0300$, $\beta = 0.0180$, $\theta_{10} = \theta_{20} = 0$. The orbit constructed also lasts 624 years. Due to the relations expressed by the second term in Eq. (73), α and β are coupled and β is actually solved from α by Eq. (73). Generally, only when α is larger than a lower limit can the halo orbits exist (i.e. Eq. 73 is solvable). For the point L_1, this lower limit is around 0.0160. For the point L_2, this lower limit is around 0.0300. For the orbit in Fig. 14, the time interval between consecutive nodal points is 0.8 dimensionless units and totally 65537 nodal points are used. For the orbit in Fig. 15, the time interval is 0.4 dimensionless units and totally

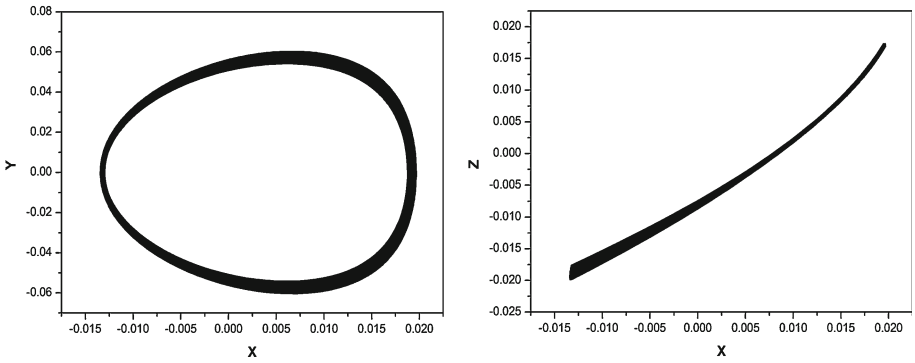

Fig. 14 One halo orbit around the point L_1, lasting 624 years

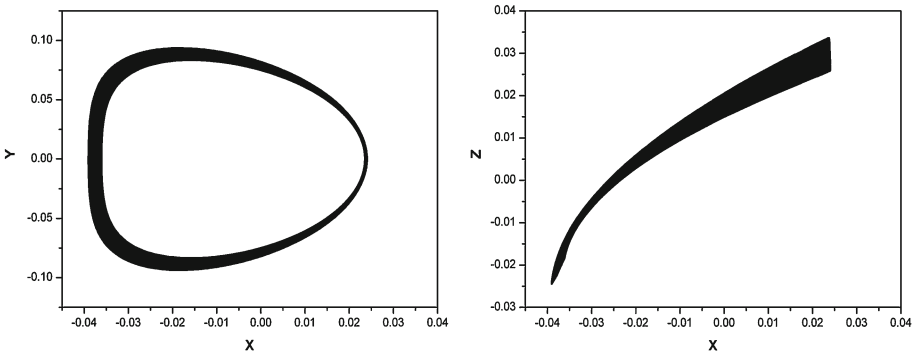

Fig. 15 One halo orbit around the point L_2, lasting 624 years

Table 6 Coefficients in the frequencies v_1, d for the halo orbit

Frequency	v_i^{20}	v_i^{02}	v_i^{40}	v_i^{22}	v_i^{04}
$L_1 - v_1$	−185.2783	8.4746	990.7485	146.5610	239.7349
$L_1 - d$	280.2466	−23.4266	−12529.4052	4019.8616	−485.1700
$L_2 - v_1$	−23.6111	9.3625	−2390.0498	−348.2373	219.2830
$L_2 - d$	86.2530	−12.0640	−197.1637	2922.8657	−322.0514

131073 nodal points are used. Similarly, we only list the coefficients of the frequencies for readers to check the results (see Table 6).

5.3 Convergence of the literal series

An interesting phenomenon is that the literal expansions of the Lissajous orbit and the halo orbit constructed in this paper are divergent for large amplitude motions. However, for the same amplitude, literal expansions in the CRTBP model are not divergent (Gómez et al. 2001c; Jorba and Masdemont 1999). As an example, we take the halo orbit around the point L_1 to state the problem and explain it.

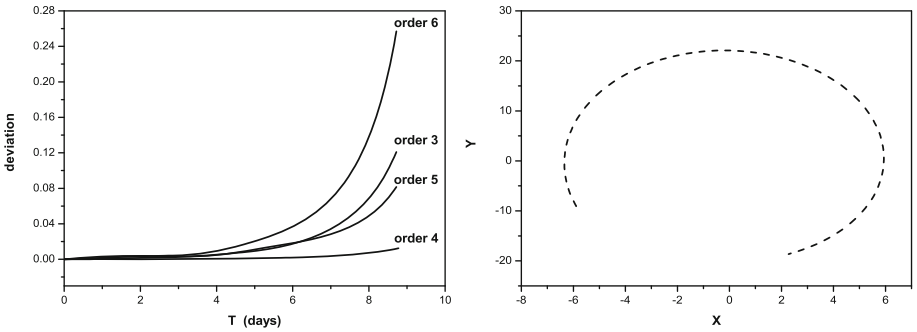

Fig. 16 The *left frame* shows the deviation between the analytic solution of the halo orbit and the numerically integrated orbit, for different orders. The *right frame* shows the analytic solution of the order 7

We manage to construct the analytic solution up to the order 7. The left frame of Fig. 16 shows the deviation curve of the state vectors between the analytic solution and the integrated orbit. The initial conditions of the two orbits are the same. Judging from the figure, we know the convergence reaches its best for the analytic solution of order 4. For analytic solutions of the order larger than 4, the divergent speed increases with the order. For the analytic solution of order 7, the right frame of Fig. 16 shows the analytic orbit. Judging from the size of the orbit, we know that it can not even be called a halo orbit anymore.

The reason for this phenomenon lies in the resonances between the basic frequencies $\omega_1, \omega_2, \omega_3, \omega_4$ and the basic frequency v_1, which is a common phenomenon in dynamical systems. Briefly speaking, a set of integers exist such that

$$\omega = i\omega_4 + j\omega_1 + k\omega_2 + l\omega_3 + mv_1 \to 0 \tag{77}$$

In the case of resonances, the well-known small denominator problem will cause the divergence of the literal series (Siegel and Moser 1971).

For the halo orbit in the CRTBP, there is only one basic frequency, so there are no such problems. The literal series converges as long as the expansion of the force functions in Eq. (58) converges. For the Lissajous orbit in the CRTBP, although such problems also exist, the small denominator appears only for very high orders due to the fact there are only two basic frequencies other than six in the real Earth–Moon case.

For the point L_2, similar resonance problems exist, as reported in Andreu (1998). However, the existence of the small denominator problem doesn't mean that no invariant curves (in our case, Lissajous orbits and halo orbits) exist. It just means that we can not construct literal solutions this way. Maybe other methodologies should be taken, just as the proof history of the well-known KAM theory (Siegel and Moser 1971).

6 Conclusions

The dynamical substitutes of the three collinear libration points in the real Earth–Moon system were computed. They are unstable but with central manifolds around them. For the points L_1 and L_2, linearized motions around the dynamical substitute were firstly obtained and then higher order analytical solutions of the central manifolds were constructed. Taking the higher order analytical solutions as initial seeds of the parallel shooting method, quasi-periodic orbits including Lissajous orbits and halo orbits were constructed.

Acknowledgments This work is supported by the national Natural Science Foundation of China (NSFC 10903002, 40974019, 11078001). The second author is also supported by NSFC 11033099, 11003009. The authors thank the anonymous reviewers for their valuable comments to improve the paper.

Appendix

We prove here why $p_{1c,m'n'}^{000010} = p_{2s,m'n'}^{000010} = 0$ in Eq. (30). Similar discussions go for Eq. (31), (38) and (39).

Extract all the terms with the angle θ in y_1 and y_2. According to the construction rules stated in the text, these terms should satisfy

$$\begin{cases} (y_1)_\theta = \left(\alpha + y_1^{high}\right)\cos\theta \\ (y_2)_\theta = \alpha \sin\theta \end{cases}, \tag{A1}$$

where y_1^{high} means higher order terms in the solution. The frequency v_1 can be expressed as $v_1 = v_1^{00} + v_1^{high}$. Taking the above equation back to Eq. (18), we have

$$\begin{cases} 0 = [B^{-1}O(\Delta X^2)]_{1c} \\ -\left(v_1^{00} + v_1^{high}\right)\left(\alpha + y_1^{high}\right) + v_1^{00}\alpha = [B^{-1}O(\Delta X^2)]_{1s} \\ \left(v_1^{00} + v_1^{high}\right)\alpha - v_1^{00}\left(\alpha + y_1^{high}\right) = [B^{-1}O(\Delta X^2)]_{2c} \\ 0 = [B^{-1}O(\Delta X^2)]_{2s} \end{cases}. \tag{A2}$$

Obviously,

$$[B^{-1}O(\Delta X^2)]_{1c} = \sum_{m'n'} \alpha^{m'}\beta^{n'} p_{1c,m'n'}^{000010}, \quad [B^{-1}O(\Delta X^2)]_{2s} = \sum_{m'n'} \alpha^{m'}\beta^{n'} p_{2s,m'n'}^{000010}. \tag{A3}$$

This relation holds for all α, β. Thus $p_{1c,m'n'}^{000010} = p_{2s,m'n'}^{000010} = 0$.

References

Andreu, M. A. : The quasi-bicircular problem. PhD Thesis, Department of Matemàtica Aplicada i Anaàlisi, Universitat de Barcelona (1998)

Arnold, V.I.: Mathematical Methods of Classical Mechanics. 2nd edn. Beijing World Publishing Corporation, Beijing (1999)

Broschart, S.B. et al.: Preliminary trajectory design for the Artemis lunar mission. In: Astrodynamics Specialist Conference, No AAS 09-382. Pittsburgh, Pennsylvania, 9–13 August (2009)

Brouwer, D., Clemence, G.M.: Methods of Celestial Mechanics. Academic press, New York (1961)

Díez, C., Jorba, À., Simó, C.: A dynamical equivalent to the equilateral libration points of the Earth–Moon system. Celest. Mech. Dyn. Astron. **50**, 13–29 (1991)

Dunham, D.W., Farquhar, R.W.: Libration point missions, 1978–2002. In: Gómez, G., Lo, M.W., Masdemont, J.J. (Eds.) Proceedings of the Conference on Libration Point Orbits and Applications, pp. 45-73. World Scientific, Singapore (2003)

Farrés, A., Jorba, Á.: Periodic and quasi-periodic motions of a solar sail close to SL_1 in the Earth-Sun system. Celest. Mech. Dyn. Astron. **107**, 233–253 (2010)

Folda, D., Vaughn, F.: A survey of Earth–Moon libration orbits: stationkeeping strategies and intra-orbit transfers. In: AIAA 2004-4741, AIAA/AAS Astrodynamics Specilist Conference, Providence, Rhode Island (2004)

Gómez, G., Llibre, J., Martínez, R., Simó, C.: Dynamics and Mission Design near Libration Point Orbits, Vol. I, Fundamentals: The Case of Collinear Libration Points. World Scientific, Singapore (2001a)

Gómez, G., Jorba, À., Masdemont, J., Simó, C.: Dynamics and Mission Design near Libration Point Orbits, Vol. III, Advanced Methods for Collinear Points. World Scientific, Singapore (2001b)

Gómez, G., Llibre, J., Martínez, R., Simó, C.: Dynamics and Mission Design near Libration Point Orbits, Vol. II, Fundamentals: The Case of Triangular Libration Points. World Scientific, Singapore (2001c)
Gómez, G., Jorba, À., Masdemont, J., Simó, C.: Dynamics and Mission Design near Libration Point Orbits, Vol. IV, Advanced Methods for Triangular Points. World Scientific, Singapore (2001d)
Gómez, G., Masdemont, J.J., Mondelo, J.M.: Solar system with a selected set of frequencies. Astron. Astrophys. **390**, 733–749 (2002)
Hou, X.Y., Liu, L.: On quasi-periodic motions around the triangular libration points of the real Earth–Moon system. Celest. Mech. Dyn. Astron. **108**, 301–313 (2010)
Jorba, À., Ramírez, R., Villanueva, J.: Effective reducibility of quasi-periodic linear equations close to constant coefficients. SIAM J. Math. Anal. **28**(1), 178–188 (1997)
Jorba, À., Simó, C.: On quasi-periodic perturbations of elliptic equilibrium points. SIAM J. Math. Anal. **27**(6), 1704–1737 (1996)
Jorba, À., Masdemont, J.: Dynamics in the centre manifold of the collinear points of the restricted three body problem. Physica D **132**, 189–213 (1999)
Lichtenberg, A.H., Lieberman, M.A.: Regular and Stochastic Motion. Springer, New York (1983)
Murray, C.D., Dermott, S.F.: Solar System Dynamics. Cambridge University Press, Cambridge (1999)
Romagnoli, D., Circi, C.: Lissajous trajectories for lunar global positioning and communication system. Celest. Mech. Dyn. Astron. **107**, 409–425 (2010)
Siegel, C.L., Moser, J.K.: Lectures on Celestial Mechanics. Springer, Heidelberg (1971)
Szebehely, V.: Theory of Orbits. Academic Press, New York (1967)